Merging modelled and reported flood impacts in Europe in a combined flood event catalogue, 1950-2020

Dominik Paprotny[1], Belinda Rhein[1,2], Michalis I. Vousdoukas[3], Paweł Terefenko[4], Francesco Dottori[5], Simon Treu[1], Jakub Śledziowski[4], Luc Feyen[6], and Heidi Kreibich[7]

[1] Potsdam Institute for Climate Impact Research (PIK), Member of the Leibniz Association, P.O. Box 60 12 03, 14412 Potsdam, Germany, [2] Humboldt-Universität zu Berlin, Berlin, Germany, [3] University of the Aegean, Department of Marine Sciences, Mytilene, Greece, [4] Institute of Marine and Environmental Sciences, University of Szczecin, Adama Mickiewicza 16, 70-383 Szczecin, Poland, [5] CIMA Research Foundation, Savona, Italy, [6] European Commission, Joint Research Centre (JRC), Ispra, Italy, [7] GFZ German Research Centre for Geosciences, Section Hydrology, Potsdam, Germany

Correspondence to: Dominik Paprotny (dominik.paprotny@pik-potsdam.de)

Abstract. Long-term trends in flood losses are regulated by multiple factors including climate variation, demographic dynamics, economic growth, land-use transitions, reservoir construction and flood risk reduction measures. Attribution of those drivers through the use of counterfactual scenarios of hazard, exposure or vulnerability first requires a good representation of historical events, including their location, intensity and the factual circumstances in which they occurred. Here, we develop a chain of models that is capable of recreating riverine, coastal and compound floods in Europe between 1950 and 2020 that had a potential to cause significant socioeconomic impacts. This factual catalogue of almost 15,000 such events was scrutinised with historical records of flood impacts. We found that at least 10% of them had led to significant socioeconomic impacts (including fatalities) according to available sources. The model chain was able to capture events responsible for 96% of known impacts contained in the HANZE flood impact database in terms of persons affected and economic losses, and for 81% of fatalities. The dataset enables studying drivers of vulnerability and flood adaptation due to a large sample of events with historical impact data. The model chain can further be used to generate counterfactual events, especially related to climate change and human influence on catchments.

1 Introduction

Flood risk is constantly evolving and influenced by a wide array of drivers, related to atmospheric, land surface and socio-economic processes (Merz et al., 2021). Recent decades have been identified as a particularly flood-rich period along European rivers (Blöschl et al., 2020) and increasing sea levels are expected to exacerbate coastal flood risk (Vousdoukas et al., 2017, 2023, Nicholls et al., 2021). At the same time exposure is growing rapidly (Paprotny et al., 2018b, Andreadis et al., 2022, Rentschler et al., 2023) and mitigation actions are implemented in reaction to floods (Kreibich et al., 2022). Disentangling the different risk drivers requires considerable modelling effort to reconstruct the factual circumstances surrounding the occurrence of floods and modelling them again under alternative (counterfactual) conditions (Scussolini et al., 2023). Such analyses enable impact attribution, i.e. linking changes in impacts with their likely causes. It can then provide information on long-term development of risk, which in turn has implications on cost-benefit analyses or risk management planning (Kreibich et al., 2019).

The recent Sixth Assessment Report of the Intergovernmental Panel on Climate Change, in the chapter on Europe (Bednar-Friedl et al., 2022), indicated low confidence in trends in riverine and coastal flood impacts in the past half-century, even if some increase was detected for parts of the continent. The report contained very limited information on attribution, but this gap is being slowly filled by new studies. For example, Sauer et al. (2021) quantified hazard, exposure and vulnerability changes for flood events globally, finding that for Europe the increase in flood losses was driven almost entirely by exposure, with some small decline in hazard and vulnerability. Though the timeframe of the study was short (1980–2010), it highlighted the role of exposure similarly to Paprotny et al. (2018b), who presented exposure-adjusted losses for 1870–2016 (with consideration for gaps in flood impact reporting), finding no upward trend in economic losses and a strong decline in fatalities. Long-run global data on climatic and socioeconomic drivers under factual and counterfactual scenarios are available from the Inter-Sectoral Model Intercomparison Project, or ISIMIP 3a (Frieler et al., 2024), but they mostly have coarse resolution that is not easily applicable to Europe and have not yet been used for flood impact attribution. Impact attribution of European floods was also carried out with a case study-based, semi-quantitative approach of comparing "paired events", i.e. floods that have occurred in the same area some years apart (Kreibich et al., 2023). This approach has an advantage mainly in the context of drawing practical conclusions for flood adaptation (Kreibich et al., 2019). Studies that derived projections of future flood risk in Europe have indicated that all three components of risk play an important role in determining changes in the impact magnitude (Rojas et al., 2013, Vousdoukas et al., 2018, Steinhausen et al., 2022, Schoppa et al., 2024).

Particular effort is needed in reconstructing the intensity and spatial footprint of flood events. For instance, the loss-normalisation study of Paprotny et al. (2018b) used 100-year riverine and coastal flood hazard maps as proxies for impact zones within subnational regions indicated as affected in the HANZE database (Paprotny et al., 2018a). This approach did not include the effect of climate change, human influence on catchments or simply the variation in return period of different events. There have been attempts to reconstruct past river floods for North America (Wing et al., 2021) or storm surge footprints globally (Enríquez et al., 2020), but none specifically for Europe. Satellite-derived flood footprints can also be linked to impact records, as in Mester et al. (2023), but such datasets cover only a short timeframe and do not resolve the problem of generating a counterfactual hazard scenario.

In this study we develop a modelling chain to generate a factual flood catalogue for 42 European countries covering the period 1950–2020, which could be further used to run counterfactual scenarios. We only cover the factual scenarios and focus on deriving the best possible reconstruction of past riverine, coastal and compound floods. The main metric of success of the modelling chain is its ability to correctly derive the time, location and intensity of 2037 actual floods contained in the HANZE flood impact database (Paprotny et al., 2023). We further aim at deriving not only the floods that caused significant socioeconomic impacts, but also those that did not happen despite their hydrological extremity due to existing flood protection, as this could later be used to quantify the level of European flood protection.

Thanks to the availability of new high-resolution estimates of past population and economic exposure (Paprotny and Mengel, 2023), we narrow down our catalogue of floods only to those with significant socioeconomic impact potential, rather than those which were extreme only from a hydrological perspective. This enables comparison with historical records of flood impacts and classifying the modelled events in accordance to their real-life consequences (or lack thereof). Finally, the focus is on coastal, compound and slow-onset riverine flooding. Flash flood events occurring in small catchments (i.e. with an upstream area below 100 km²) are not considered in our analysis due to the insufficient resolution of the riverine flood models available for Europe. Furthermore, we explicitly omit urban floods resulting from insufficient storm drainage rather than from channel overflow.

The paper provides a short method overview in section 2.1, which is followed by details on the coastal (2.2) and riverine (2.3) components of the modelling chain, which are brought together for a final flood catalogue compared with historical records (2.4). Validation of the hydrological hazard follows in the next sections (2.5, 3.1), with an overview of risk indicators derived from the catalogue (3.2) and finally comparison between modelled and observed flood impacts (3.3). The discussion analyses the limitations and uncertainties of both the modelled (4.1) and observational data (4.2), before drawing conclusions and highlighting possible applications of the flood catalogue (section 5).

2 Methods

2.1 Overview

Simulating riverine and coastal floods requires different modelling approaches. First, we derive extreme river discharges and coastal water levels, then we apply a common approach to produce flood intensity maps, compute damages, and aggregate the results spatiotemporally. Compound floods are generated by combining the results of the two strands of modelling work, therefore we run the coastal model first, and compound floods are considered as part of the riverine component, drawing on the previous coastal results. The methodology is briefly summarised in Fig. 1.

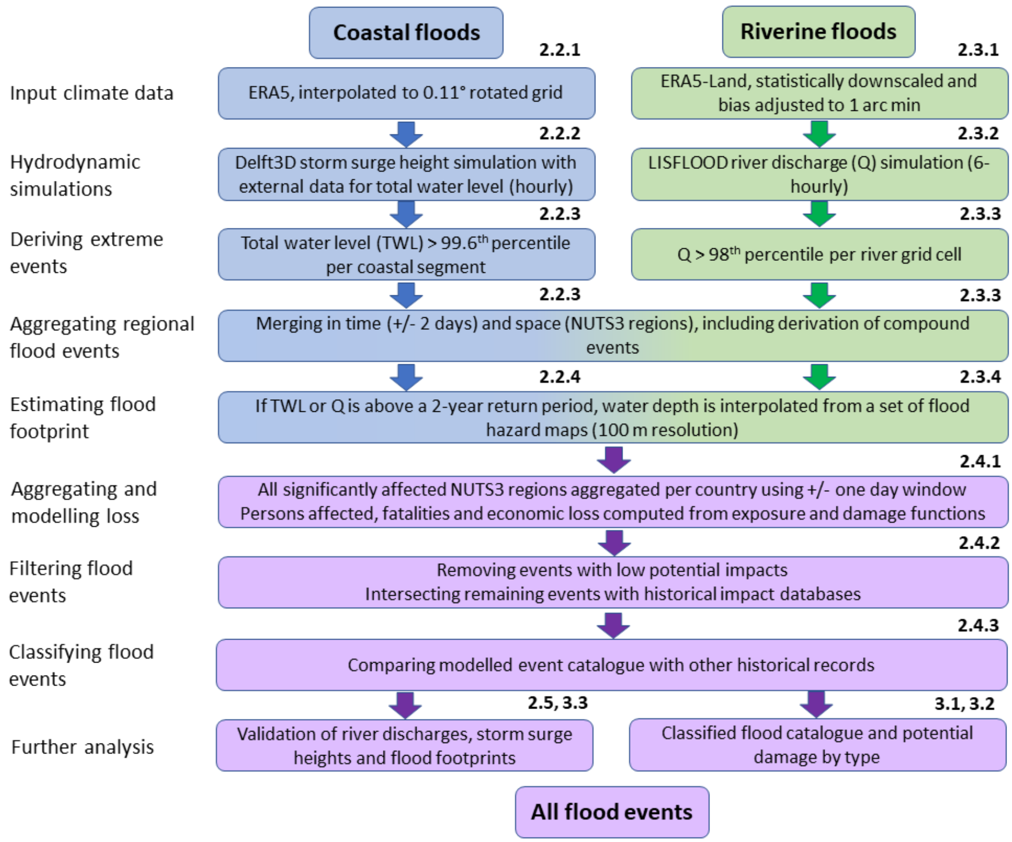

Figure 1. Workflow of the methodology, with section numbers indicated above each box.

In Fig. 1, the aggregation of extreme discharge or water levels spatially by using NUTS3 regions is mentioned. This refers to the European Union's (EU) Nomenclature of Territorial Units for Statistics (NUTS). This classification has 4 levels (0, 1, 2, 3), in which 0 is the national level and 3 is the finest sub-regional division. NUTS3 regions are usually administrative divisions, though at times statistical (analytical) regions are used instead, by amalgamating smaller administrative units (Eurostat, 2022). Due to its relevance for determining regional policy, data dissemination, and socioeconomic analyses in the EU, we use this classification as our principal unit of analysis. This further enables direct comparison with the HANZE flood impact catalogue, which contains data on 2037 reported floods in the study area since 1950, including footprints defined at NUTS3 level (Paprotny et al., 2023). HANZE also includes exposure and other subnational statistics at the same resolution (Paprotny and Mengel, 2023). The generation of a high-resolution boundary map of 1422 NUTS3 regions, version 2010, or their equivalents, is described in Paprotny and Mengel (2023). We further aggregate flood events at national level for comparison with reported impacts, as this is the typical resolution in which such information is provided. Consequently, the catalogue is not specific for river catchments or sea basins (as in e.g. Diederen et al., 2019), but for countries and their subdivisions.

It should be highlighted that the catalogue represents possible floods without considering structural flood protection measures, hence they are not included in the potential flood footprint estimates. Due to the very limited information on present or past protection standards, adding estimates of those would potentially create large inaccuracies by filtering out events that happened in history.

2.2 Coastal model

2.2.1 Climate data

We model storm surge heights driven by hourly 10-m wind speeds (*u* and *v* component) and surface air pressure, drawing data from the latest ERA5 climate reanalysis (Hersbach et al., 2020). The data were downloaded at a resolution of 0.25° (approximately 28 km at the equator) and then interpolated using first-order conservative remapping (Jones, 1999) to a 0.11° rotated-pole (12.5 km) grid used in our storm surge model, which in turn is the same as the CORDEX grid used in European climate projections (Jacob et al., 2014). Apart from the interpolation, no further adjustments were made to the data.

2.2.2 Sea level estimation

The principal component of extreme sea levels are storm surges, which we estimate through a continuous simulation in Delft3D. This hydrodynamic model is commonly applied in continental- or global-scale surge modelling (e.g. Vousdoukas et al., 2016a, Ganguli et al., 2020, Muis et al., 2020). The model set-up is the same as described in Paprotny et al. (2016, 2019), with the difference that it is forced by wind and atmospheric pressure fields from ERA5 instead of ERA-Interim. We also carried out a calibration, using the previous calibration as the starting point, by adjusting the sea bottom roughness coefficients for different basins around Europe, and comparing the modelled surge heights with tide gauge observations for years 2011–2019. This recalibration also benefited from much better availability of observational data, which are described in section 2.5, as they are also used to validate the final simulation. Additionally, the timestep of the model was reduced to 15 min, with outputs saved hourly, compared to 30 min and 6 hours, respectively, in the original version. The model was run from 1 January 1949 to 31 December 2020, with the first year used only as spin-up. Actual ERA5 data was used in the spin-up phase thanks to recent extension of the dataset to 1940.

As storm surge heights are only one component of extreme sea levels, the hourly total water level (L) is the combination of six components:

$$L = S + T + W + D + M + G \tag{1}$$

Where:

- S is the hourly storm surge height;
- T is the hourly tide elevation, computed with pyTMD package (https://github.com/tsutterley/pyTMD) from 34 tidal constituents;

- W is the hourly wave run-up, assumed to be 20% of significant wave height (recommended by U.S. Army Corps of Engineers, 2002, used e.g. in Vousdoukas et al., 2016b);
- D is the mean dynamic topography defined as the average sea surface height for 1993–2012 above geoid;
- M is the long-term variation in sea level related to climatic variation ("sea level rise", SLR), defined as average annual difference from average sea level in year 2000;
- G is the glacial isostatic adjustment (GIA) computed from long-term historical rate of change.

Each component was derived from a different source, as summarised in Table 1.

Table 1. Source of data for computing hourly total water level. * coarser global data were used for northernmost coasts of Europe

Component	Source	Spatial resolution	Temporal resolution	Reference
Storm surge height	Delft3D simulation (this study)	12.5 km	hourly	Paprotny et al. (2016)
Tide elevation	FES2014	1/16°	hourly	Lyard et al. (2021)
Wave run-up	ERA5	1/2°	hourly	Hersbach et al. (2020)
Mean dynamic topography	Global Ocean Mean Dynamic Topography (combines global CNES-CLS18 and CMEMS2020 for Black and Mediterranean seas)	1/8°	1993-2012 average	Mulet et al. (2021)
Sea level rise	1950–99: Hourly Coastal water levels with Counterfactual (HCC)	10 km	hourly (used as annual average)	Treu et al. (2024)
	2000–2020: European Seas Gridded L4 Sea Surface Heights*	1/8°	monthly (used as annual average)	Taburet et al. (2019)
	2000–2020: Global Ocean Gridded L4 Sea Surface Heights*	1/4°		Pujol et al. (2016)
Glacial isostatic adjustment	ICE-6G_C	1/5°	long-term rate of change	Argus et al. (2014), Peltier et al. (2015)

2.2.3 Extracting coastal flood events

As the resolution of each dataset that is used to derive the total water level varies, we assign the nearest grid point of each model to 5884 coastal segments defined in the coastal flood hazard model (Vousdoukas et al., 2016b) with a nearest-neighbour approach. The segments represent no more than 25 km of the coast (if completely straight), but usually about 15 km. They stretch up to 100 km inland, but far less for more complex areas such as deltas, estuaries, fjords, or islands. From the detrended (1950–2020) hourly timeseries, occurrences of water level above the 99.6th percentile were identified and considered potential coastal floods. The detrending was needed as events derived here are used for extreme value analysis (section 2.2.4). Occurrence of water levels below the 99.6th percentile for at least two full calendar days separated two events from each other. Such thresholds lead to, on average, about five potential flood events per year. Then, events were aggregated according to NUTS3 regional boundaries, again with the principle that the beginning of any segment-level flood event in a NUTS3 region has to occur at least two full calendar days after the end of any previous segment-level event in that region.

2.2.4 Deriving coastal flood footprints

For each coastal segment in the dataset, an extreme value analysis was carried out using a Generalised Pareto distribution and a peak-over-threshold approach. The analysis was carried out with Matlab function *fitdist*, using maximum likelihood estimation and the 99.6th percentile thresholds from the previous step. This enabled deriving extreme sea level scenarios (return periods of 2, 5, 10, 20, 30, 50, 100, 200, and 500 years) for coastal inundation modelling. This was carried out according to a methodology developed by Vousdoukas et al. (2016b). Briefly, the maps were generated with the Lisflood-ACC (LFP) model (Bates et al., 2010) applied at 30 m spatial resolution. In terms of Digital Elevation Model (DEM), we use the recently published GLO-30 DEM (European Space Agency and Sinergise, 2021) after applying post-processing using global LIDAR observations to further remove vertical bias, correcting for buildings and vegetation. The description of the GLO-30 post-processing is described in detail in Pronk et al. (2024). The simulations consider gridded hydraulic roughness values derived from land-use maps (Zanaga et al., 2021). Lisflood-ACC is applied for each coastal segment with the model domain extending up to 200 km landwards in order to ensure the inclusion of all potentially hydrologically connected areas that may lie inland and away from the coast.

Total water level of each segment-level flood event is linked with the water level used to generate the flood hazard maps for each segment. In this way, it is possible to interpolate water depths from the stack of hazard maps to event-specific extreme sea levels. This is only done if the water levels for an event exceed a flood threshold, defined as the higher of the two following thresholds:

- Total water level with a 2-year return period, derived from the Generalised Pareto distribution;
- Maximum observed total water level minus storm surge height.

The first threshold was chosen for consistency with the riverine model as it is akin to the typical definition of a bank-full river discharge. The second threshold was added to avoid overestimating risk in regions (mainly Eastern Mediterranean), where storm surge heights are very low, but wave run-up contributes significantly to extreme sea level.

Only grid cells with water depths of at least 10 cm were considered inundated for consistency with riverine flood maps. The individual flood maps for each coastal segment were aggregated within a NUTS3-level event. Finally, only those NUTS3-level events were preserved for further analysis if the potential flood zone was at least 100 ha. As further processing is carried out together with the riverine model, we now describe the river component, and continue explaining the next steps towards the combined flood catalogue in section 2.4.

2.3 Riverine model

2.3.1 Climate data

We used river discharge from Tilloy et al. (2024) that was modelled using ERA5-Land, which is a downscaled version of ERA5 characterised by 0.1° (approximately 11 km at the equator) resolution (Muñoz-Sabater et al., 2021). It was further statistically downscaled and bias adjusted to 1' (arc minute) resolution using ISIMIP3BASD v3.0.0 method developed by

Lange (2019, 2022), using EMO-1 gridded observational data, which is a 1' variant of the EMO-5 dataset developed by Thiemig et al. (2022). Temperature and precipitation with 6-hourly resolution were used as the primary driver of the hydrological model, while potential evapotranspiration was computed at daily resolution using the LISVAP model by van der Knijff (2006). For details on the preparation of the meteorological data, we refer to Tilloy et al. (2024).

2.3.2 River discharge simulation

Tilloy et al. (2024) modelled river discharges a through continuous simulation using the LISFLOOD hydrological model (Burek et al., 2013) implemented in the European Flood Awareness System, or EFAS (Copernicus Emergency Management Service, 2023). Tilloy et al. (2024) used the latest model set-up, v5.0 (Choulga et al., 2023), and simulated river discharges with meteorological inputs described in section 2.3.1. The EFAS model was run from 3 January 1950 to 31 December 2020 following the 71-year pre-run. Due to rapid evolution of socioeconomic conditions in the catchments of Europe, the input socioeconomic maps were changed with the start of every new calendar year of the simulation. The evolving socioeconomic conditions included land use (in six classes), reservoirs (based on the year of construction of each dam), and water demand (in four sectors). For details on the river discharge simulation and its validation, we again refer to Tilloy et al. (2024).

2.3.3 Extracting riverine flood events

From Tilloy et al. (2024) we derived a time series of 6-hourly discharge for 7.5 million grid cells. Due to the availability of flood hazard maps for footprint estimation (section 2.3.4), we extract data only for 282,528 grid cells that have an upstream area of at least 100 km². Occurrences of discharge above the 98th percentile (on annual basis) were identified and considered potential riverine floods. Occurrence of water levels below the 98th percentile for at least two full calendar days separated two events from each other. As in the coastal model (section 2.2.3), those thresholds were intended to produce roughly five potential flood events per year in each grid cell. Then, events were aggregated according to NUTS3 regional boundaries, again with the principle that the beginning of any grid cell-level flood event in a NUTS3 region has to occur at least two full calendar days after the end of any previous grid cell-level event in that region.

2.3.4 Deriving riverine and compound flood footprints

For each grid cell in the dataset, an extreme value analysis was carried out using a Generalised Pareto distribution and a peak-over-threshold approach, where the peak discharge was detrended based on annual maximum discharge for 1950–2020. The analysis was carried with Python package *SciPy*, using maximum likelihood estimation and the 98th percentile thresholds from the previous step. In contrast to the coastal model (section 2.2.4), no additional hydrodynamic modelling was carried out in the riverine model. Instead, the flooding processes were represented using the dataset of flood hazard maps developed by Dottori et al. (2022), which are available for a range of return periods from 10 to 500 years for grid cells with an upstream area above 500 km² . The maps were generated with the Lisflood-ACC (LFP) model (Bates et al., 2010), applied at 100 m spatial resolution and driven by hydrological simulations from a previous set-up of EFAS (Arnal et al., 2019). In this study, given the different resolutions of the LISFLOOD simulations and the flood hazard maps, the two datasets were matched according to the procedure described in Dottori et al. (2022).

To provide coverage for smaller catchments, the flood maps by Paprotny et al. (2017) were applied for grid cells with an upstream area of 100–499 km². The maps for five scenarios (return periods of 10, 30, 100, 300 and 1000 years) were based on discharges estimated with a Bayesian Network-based model from Paprotny and Morales-Nápoles (2017). The simulations were performed using a one-dimensional 'steady-state' hydraulic model Deltares SOBEK to obtain water levels along rivers. Those levels were then used to generate water depth maps over a digital elevation model. The maps use the exact same grid as the ones from Dottori et al. (2022). For details on the methodology and validation of the maps we refer to Paprotny et al. (2017).

Peak river discharge per each grid cell during a given potential river flood event was linked with the scenarios used to generate the flood hazard maps so that the appropriate maps were used to interpolate water depths. If the return period of the peak discharge was below 10 years, water depths were extrapolated using two maps with the lowest return periods. No flooding was assumed if the peak discharge was below the empirical 2-year return period derived from detrended 1950–2020 peak discharges of the extracted flood events. This threshold was typically much lower than the 2-year return period derived with the Generalized Pareto distribution. Due to the logarithmic nature of the relationship between river discharge and water level, we used the natural logarithm of discharge as basis of interpolation. The maps have different extents, therefore if an area is not flooded in the map with a lower return period, the interpolation is between zero depth and water depth of the map with a higher return period is made.

Only grid cells with water depths of at least 10 cm were considered inundated, as in the maps of Dottori et al. (2022). The individual flood maps for each river grid cell were aggregated within a NUTS3-level event. Finally, only those NUTS3-level events were preserved for further analysis if the potential flood zone was at least 100 ha. At this point, the list of NUTS3-level events was compared against the same list from the coastal model. If a river event in a given NUTS3 region occurred at the same time as a coastal event in the same region, a separate "compound" event was created by merging the flood zones of the coastal and riverine events in that region. The compound events are analysed in addition to the individual coastal and riverine events, rather than replacing them. From here, processing of the potential flood events follows a common path for all types of events.

2.4 Combined flood catalogue

2.4.1 Aggregating and estimating potential losses per event

Almost 250,000 potential flood events at the level of NUTS3 regions are aggregated for each country. One full calendar day separates two country-level events consisting of at least one NUTS3 event. Coastal, riverine, and compound events are each aggregated separately. Each event is characterised by hydrological parameters, such as inundated area, average water depth, duration and return period. The latter is the geometric average of all river grid cells or coastal segments that contribute to the flooded area.

Potential losses were estimated by multiplying exposure for each 100 m grid cell within each flood footprint with an appropriate loss function. Exposure per grid cell (population and value of fixed assets) was computed with the HANZE v2.0 exposure model (Paprotny and Mengel, 2023), which estimates historical exposure changes using a combination of rule-based and statistical modelling that enabled downscaling past demographic and economic trends at subnational level into a high-resolution grid. The model provides annual data for years 2000–2020 and 5-yearly timesteps for 1950–2000. Alongside population, the model can generate values of tangible fixed asset stock in euros (constant 2020 prices and exchange rates) in 8 sectors (housing, consumer durables, agriculture, forestry, industry, mining, services, infrastructure).

Firstly, fatalities were estimated per each 100 m grid cell by multiplying the population with the death probability determined by water depth. Due to the lack of velocity data or dike breach locations, only such a simplified approach can be used here. We opted for the S-shaped depth-fatality function by Boyd et al. (2005) as presented in Jonkman et al. (2008), which shows very low chance of death until water depths of approximately 3 m, i.e.:

$$F_D = \frac{0.34}{1 + exp(20.37 - 6.18d)} \quad (2)$$

where F_D is the mortality rate and d is the water depth in m.

The second indicator, people affected, is simply the total population within the flood footprint. Finally, economic losses were estimated using a set of depth-damage functions for different economic sectors. We applied the logarithmic-type functions proposed for Europe by Huizinga et al. (2017) that distinguish five sectors: agriculture, industry, commercial, infrastructure, and residential. The functions were applied to the appropriate sector in the exposure model. It should be noted that whenever “economic losses” are mentioned in this paper, they only refer to direct damage to tangible fixed assets, without considering indirect impacts.

2.4.2 Obtaining the final flood catalogue

Estimated flood impacts of each event computed in the previous step were used to further filter the flood event catalogue only to those floods with significant potential for socioeconomic impacts. To qualify for the list, the event had to pass two thresholds simultaneously (Table 2):

- Inundated area above a fixed threshold, and
- At least one of two socioeconomic impact indicators (computed according to section 2.4.1):
    - people potentially affected above fixed threshold, or
    - potential economic losses above an event-specific threshold.

The exact threshold depends on the type of event, and in case of economic losses also on country and year of event, as it was linked to the level of gross domestic product (GDP) per capita (Table 2).

Table 2. Thresholds for selecting flood events with significant potential impacts and number of filtered events.

Threshold	Coastal floods	Riverine floods	Compound floods
Threshold			
Area inundated	1000 ha	2000 ha	
People affected	2500	5000	
Economic damage	10,000 times GDP per capita (country and year of event)	20,000 times GDP per capita (country and year of event)	
Number of events by modelling step			
Regional-level aggregated events	22,446	213,517	5235
National-level aggregated events	4208	19,918	1452
Filtered events by impact thresholds	2436	11,205	1058

Thresholds in Table 2, as well as those described earlier in the methodology, were selected iteratively based on the following objectives:

- Maximise the number of modelled events matching observed events from HANZE;
- Maximise the share of one-to-one relationships between modelled and observed events (as opposed to many-to-one or one-to-many relationships);
- Minimise the spatial extent of events in terms of affected NUTS3 regions beyond those indicated in HANZE;
- Create a list of events large enough for statistical analyses and small enough to allow manual searches of historical records for all events.

To help select the thresholds, observed flood events from the following six datasets were matched per country according to start and end dates:

- HANZE v2.1 (Paprotny et al., 2023);
- EM-DAT (Centre for Research on the Epidemiology of Disasters 2023);
- EEA Flood Phenomena (from 1980 only) (European Environment Agency, 2015);
- Dartmouth Flood Observatory (from 1985 only) (Brakenridge, 2023);
- FFEM-DB (from 1980 only) (Papagiannaki et al., 2022);
- Recorded Flood Outlines (England only) (Environment Agency, 2023).

In addition, the HANZE dataset was matched with events below the tested thresholds. Following the above objectives results in different potential impact thresholds for coastal and riverine floods. In total, some 43% of events were filtered out (Table 2).

2.4.3 Comparing modelled and reported events

The modelled flood events of the catalogue were evaluated using gauge records and impact data as well as manual research involving all kinds of documentary sources. At first, English-language papers and local-language flood catalogues providing an overview of the hazard in the country were consulted. Then, national disaster databases were searched and the relevant data was extracted. Papers on case studies of disasters were searched for in both English and the local language of the country being researched. A keyword-based search in both English and the local language was performed using a web engine to identify news articles or other online reports mentioning the relevant disasters. In total, 946 major text or data sources were used, 828 of which are listed in the HANZE v2.1 dataset (Paprotny et al., 2023) and the remainder is listed together with the data from this study. Based on this information on impacts, each event was categorised into one of the classes listed in Table 3.

Table 3. Classification of flood events considering the availability of data sources as well as reported hydrological and socioeconomic impacts. All classes are included in the final flood catalogue.

Class	Short name	Evaluation result	
		Extreme hydrological event	Inundation with significant socioeconomic impacts
A	Impacts, data	Confirmed by sources	Confirmed by sources (impact data available)
B	Impacts, no data	Confirmed by sources	Confirmed by sources (impact data not available)
C	No impacts	Confirmed by sources	Not confirmed by sources
D	Unknown impacts	Confirmed by sources	No sources available
E	False positive	Not confirmed by sources	Not confirmed by sources or no sources available
F	No information	No sources available	No sources available

In applying the classification from Table 3, a decision graph from Fig. 2 was used. In general, in case of complete lack of gauge data or documentary sources, the event was labelled F (“No information”), meaning that no observational data is available and therefore modelled data can be neither confirmed or rejected. In case gauge records are available, it was firstly evaluated if they indicate extreme values. Exceedance of a 2-year return period was considered sufficient to confirm that the modelled event was an extreme hydrological event in real life. If the threshold was not exceeded at any of the available gauge stations, the time series was analysed, and the event was considered confirmed as hydrologically extreme if a flood wave was clearly visible at the dates indicated by the model. If no flood wave was visible, the event was considered a “False positive” (label E), i.e. an error of the model that indicates a too high simulated river discharge or sea level. In rare cases, this classification was overridden if documentary sources indicated the occurrence of a flood event. It should be noted that “false positives”, like all other classes, are maintained in the final flood catalogue, so that the users of the data could decide whether include them in their analyses or not.

For events confirmed as hydrologically extreme, further analysis concentrated on the occurrence of significant socioeconomic impacts. Here, significant impacts were defined as in the HANZE database (Paprotny et al., 2023), i.e. exceedance of at least one the following thresholds:

- At least 1000 ha (10 km²) inundated;
- At least one person killed or missing presumed dead;

- At least 50 households or 200 people affected, defined preferably as affected by their homes being inundated by floodwaters, or who were evacuated from the inundated area, if the preferred statistic was not available;
- Losses in monetary terms corresponding to at least 1 million euro in 2020 prices.

In case no further information was available, the event was labelled D ("Unknown impacts"). If despite good coverage of sources (e.g. comprehensive local/national flood databases or catalogues), no impacts are mentioned, or in rare cases, direct statement that e.g. a flood emergency did not result in breaching of flood defences, the event was labelled C ("No impacts"). Also, if data on impacts were available, but they did not pass any of the aforementioned thresholds, the event was labelled as "No impacts". Events with sufficient information on significant impacts were labelled A ("Impact, data") and incorporated into the HANZE database. However, if statistical data was not accessible, or referred only to a small part of the impacted area, but available descriptions strongly indicated that one of the impact thresholds was likely exceeded, the event was recorded in a separate list of events, labelled B ("Impact, no data"). Available historical information was collected for such an event in a database that is a simplified version of HANZE. Detailed description of the data collected in this database, which is made publicly available with this study, is provided in Appendix A1. It should be noted that a matching of dates and country with historical events was not enough to label the event A or B. For that, at least one NUTS3 region affected during the event had to be correctly identified by the model.

Additional provisions were made for compound events. If a potential 'compound' flood is indicated in the catalogue, but based on reports and observations impacts can be attributed only to a coastal flood, the compound event was labelled C ("No impacts"), the corresponding coastal event as A or B, and the corresponding riverine event as C. The same approach was used if only the riverine driver was responsible for impacts. Also, if a single-driver event was found to be a "false positive" (label E), the corresponding compound event was also classified as "false positive". In this way, the compound flood definition for events labelled A and B is consistent with the HANZE database, where the interaction of coastal and riverine components is required for a flood to be classified as compound.

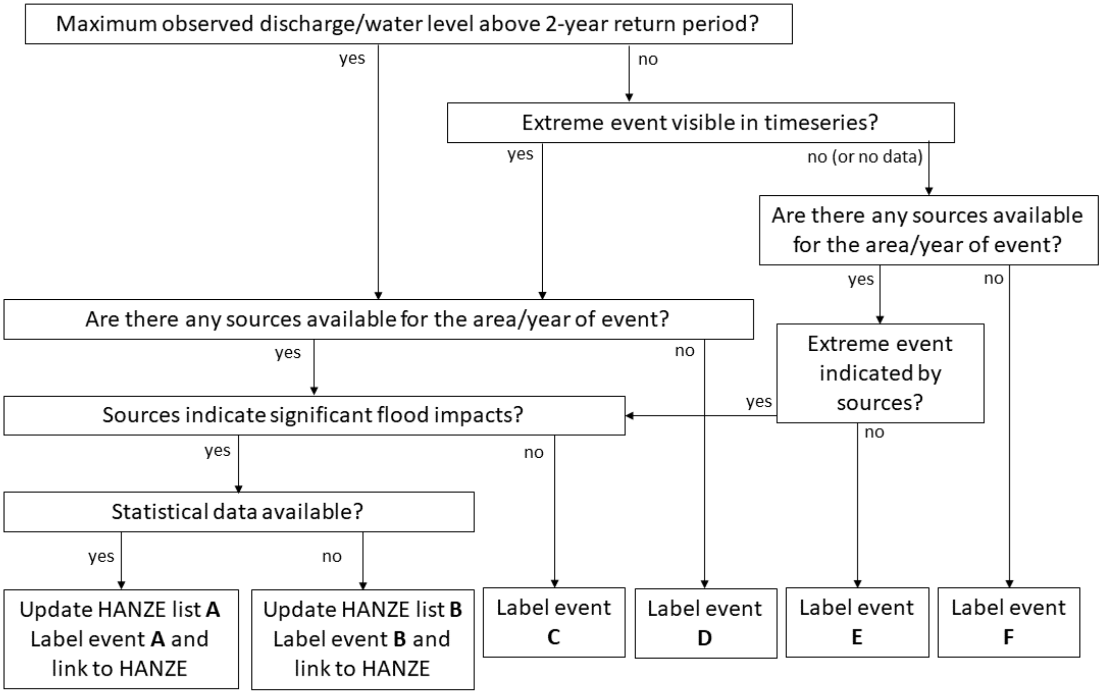

Figure 2. Decision graph for classifying flood events.

The final flood catalogue consists of two components: (1) a table with all events, indicating their timing, location, potential impacts, hydrological parameters and classification, and (2) potential flood footprint maps in vector format. The data contained in the table are explained in Appendix A2.

2.5 Validation

Validation of river discharges is presented by Tilloy et al. (2024), however we used the 3442 stations containing daily observations collected for that study for further analysis. The dataset helped us to classify the events in section 2.4.3. Further, we compared extreme discharges observed during riverine and compound events with modelled discharges. Station data was obtained in 60% from the Global Runoff Data Centre and in 40% from national public datasets of France, Norway, Poland, Spain, Sweden and the United Kingdom. The analysis was limited to 2914 stations with an upstream area of at least 100 km², located in the affected NUTS3 regions according to the model. If the event duration and available gauge series were both at least 30 days, the daily discharge was compared using the Kling–Gupta efficiency, or KGE (Gupta et al., 2009), and Spearman's coefficient of determination (as Pearson's is used in the KGE score). Otherwise, an equal amount of days was added before and after the event, so that at least 30 observations are used. The maximum daily discharges during the event were also compared.

Validation of the hourly storm surge heights, tide elevations and combined water level was done using 428 tide gauges. Almost all stations (413) were gathered from GESLA v3 dataset (Haigh et al., 2023), but for better coverage of the eastern Mediterranean Sea it was complemented with 7 stations from Poseidon System (2023), and for the southern Baltic Sea with 8 stations from the Institute of Meteorology and Water Management – National Research Institute (2023). Apart from validation for all available time series, an event-based validation was done as for river discharges. The default time window for the comparison between modelled and observed data was 7 days, unless the event had a longer duration.

Finally, the modelled flood footprints were compared with satellite-derived footprints from the Global Flood Database (GFD, Tellman et al., 2021). The footprints were converted into vector layers, with permanent water bodies removed from them, as per data contained in GFD. Only footprints within NUTS3 regions indicated as affected in the HANZE database were included in the analysis. Population affected within the footprints was derived from HANZE population maps. Flooded area and population affected based on footprints from this study and GFD were compared with reported impacts. Additionally, all flood events in the catalogue with comparative reported impact data were analysed for the difference in modelled and reported impacts. Ideally, all modelled impacts should be higher than what was reported, as the intention of the catalogue is to generate potential footprints that do not consider flood protection. Finally, footprints from this study and GFD were intersected to derive the hit rate, i.e. share of the satellite footprints correctly reproduced by the model. This is a similar approach that was used to validate flood hazard maps that are the basis of the modelled footprints (Vousdoukas et al., 2016b, Paprotny et al., 2017, Dottori et al., 2022).

3 Results

3.1 Flood event catalogue

3.1.1 Modelled impacts by classification

The final catalogue includes 2436 coastal, 11,205 riverine, and 1058 compound events with significant potential for socioeconomic impacts (Fig. 3). This already indicates a significant proportion of coastal and riverine events might be compound events. The spatial location and timeframe of events was matched with at least some gauge observations for 63% of coastal and 72% of riverine events. By applying the 2-year return period threshold to observational data, it was possible to immediately confirm that 40% of coastal and 45% of riverine events were hydrologically extreme. Further confirmations were obtained through analysis of gauge timeseries and documentary records, increasing the confirmation rate to 80% for coastal, 77% for riverine, and 66% for compound events. On the other hand, no extreme event was indicated by gauge or documentary sources for a small part of the catalogue. The false positive ratio (“E” events to “A”-“D” events) amounts to only 2.2% (16) for compound, 3.3% (67) for coastal, and 5.2% (474) for riverine floods.

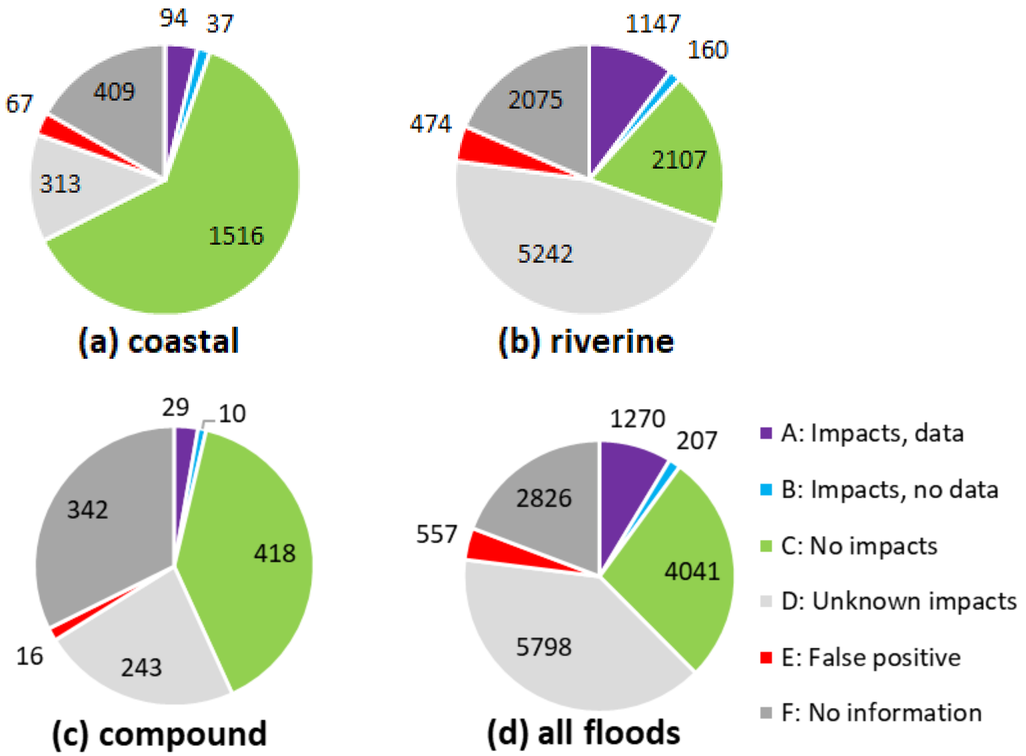

Figure 3. Flood events in the catalogue by classification: (a) coastal, (b) riverine, and (c) compound. Panel (d) shows totals for all events.

Confirmation, or at least high confidence based on available documentary sources, whether the event did, or did not, result in significant socioeconomic impacts was possible for the majority of coastal and compound events, but not for riverine floods. However, the latter occurred by far most frequently, and it was possible to confirm significant socioeconomic impacts for 11.7% of riverine (1307), 5.4% of coastal (131), and 3.7% of compound (39) events (Fig. 3). In some cases, "A" ("Impacts, data") events correspond to more than one reported flood in the HANZE database, or the events are a combination of "A" and "B" ("Impacts, no data")-type events. Therefore, the 1270 "A" and 207 "B" events actually correspond to 1471 historical floods in HANZE and 237 historical floods without impact data collected in a separate dataset as part of this study (see Appendix A1). This statistic excludes a small number of events that were below the significant impact threshold, but indicated a temporal match with the HANZE database. Only 109 such events were identified, of which only two were coastal events and two were compound events. Out of those, only 33 events, all riverine, were spatially matched with HANZE, a single historical flood in each case. This constitutes only 2% of matched HANZE events, hence we can deem the hydrological and socioeconomic thresholds in this study as well designed, as few HANZE events were missed due to their imposition without creating too many non-impact events. Also, while there were many one-to-many matches between our model and HANZE, largely due to the data-availability rules causing splitting of some flood events in HANZE, there were only a handful of cases of many-to-one connections.

The distribution of events over time (Fig. 4) shows an upward trend, which in case of “A” and “B” events is largely related to better availability of data. There is also better confidence in non-occurrence of impacts for coastal and compound events in recent decades compared to the beginning of the timeseries. An increase in “F” events in the final few years for riverine and compound events is primarily connected will lower availability of recent river gauge data.

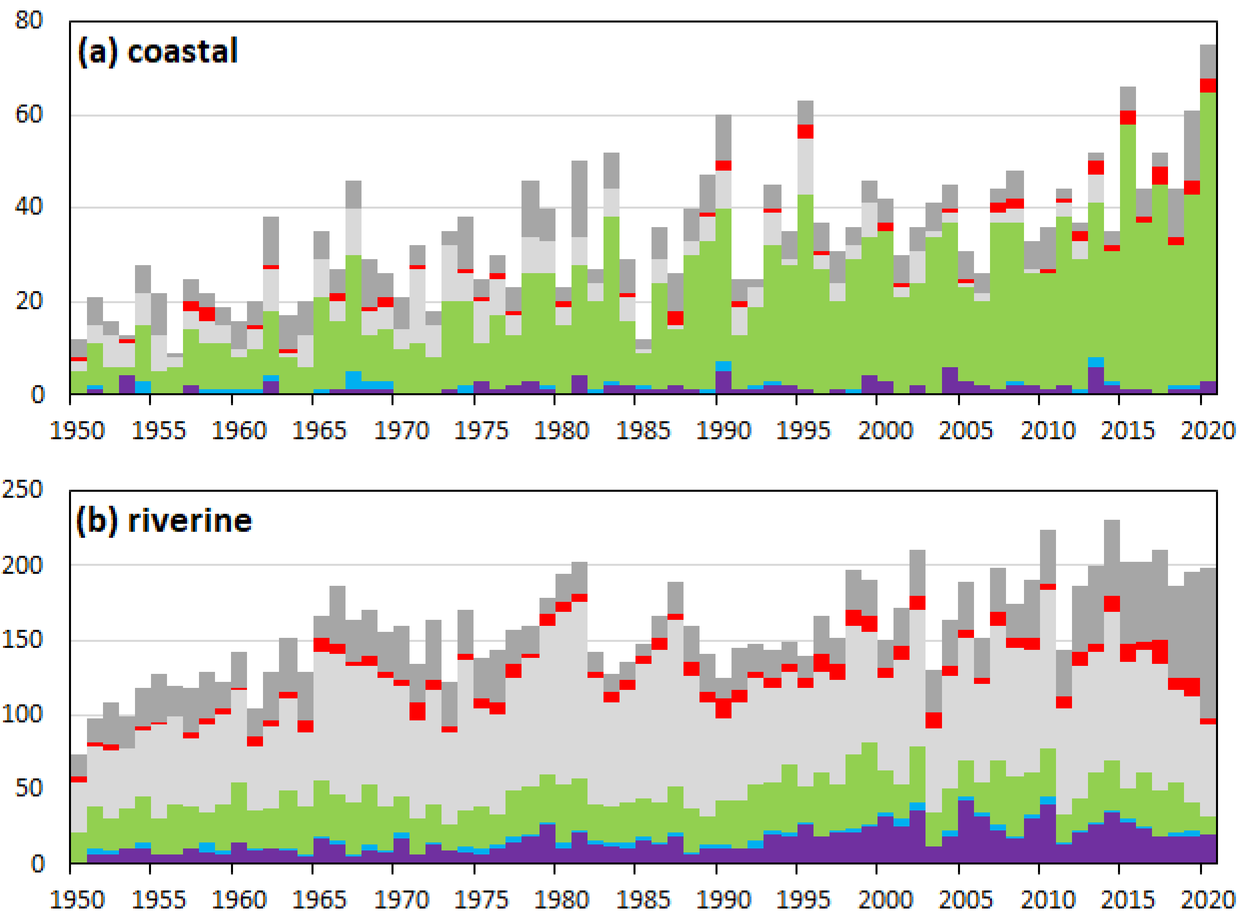

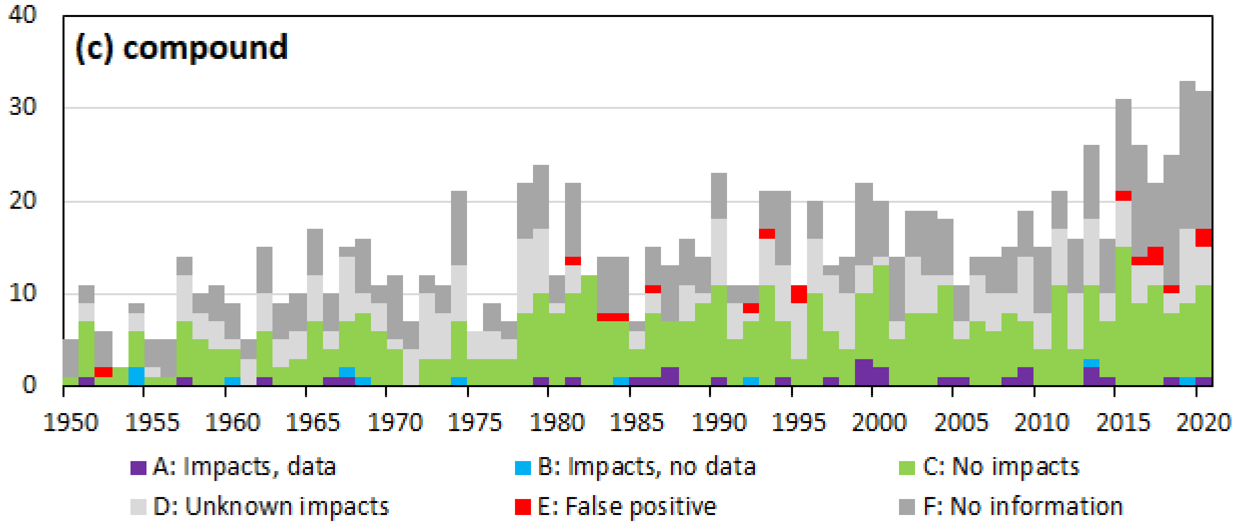

Figure 4. Flood events in the catalogue by year and classification: (a) coastal, (b) riverine, and (c) compound.

Modelled extremity and impacts of events vary strongly by class (Fig. 5). The return period along affected river and coastal segments is generally much higher for “A” and “B” events compared to all others. 18% of coastal and 37% of riverine events, in which the geometric average of return periods in the affected area was above 25 years, was classified as either “A” or “B”. In contrast, when the return period was below 5 years, the values were 2% and 10%, respectively. Interestingly, the occurrence of “F” class (“No information”) was only slightly lower for higher return periods. Confirmed impactful events were also longer in duration than other classes, with false positives (“E”) having the shortest duration. Consequently, the “A” and “B” events had, on average, the highest impact potential. In Fig. 5c, the dimensionless damage index is the average of four impact categories (potential area inundated, fatalities, persons affected, and economic loss) relative to maximum impact of any event in the country during 1950–2020 at constant 1950 exposure. False positives had, on average, the lowest impact potential. In all examples, the remaining categories (“C” – No impacts, “D” – Unknown impacts, and “F”) oscillated around the average values for all variables analysed in Fig. 5.

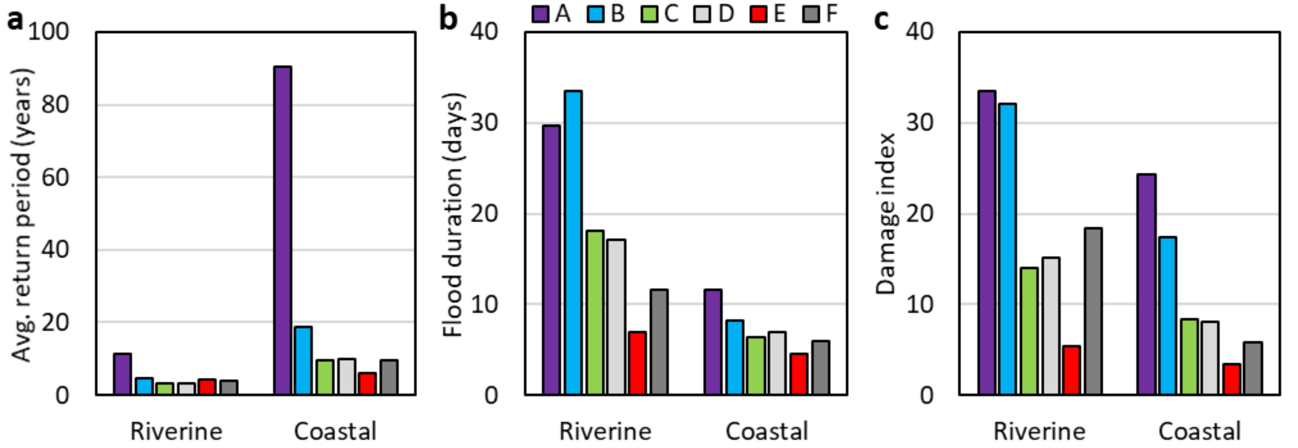

Figure 5. Comparison of mean values of selected indicators by main flood type and classification: (a) average return period along affected river or coastal segments, (b) total flood event duration, (c) dimensionless damage index, where 100 equals the highest potential impact of any event in the country during 1950–2020 at constant exposure.

3.1.2 Comparison with HANZE reported impacts database

The flood catalogue includes the majority of reported historical floods with significant socioeconomic impacts since 1950 contained in the HANZE v2.1 database (Paprotny et al., 2023). However, there is a strong difference between the completeness of the catalogue according to flood type. While about 90% of coastal, compound and slow-onset riverine floods were modelled, only 55% of flash floods were captured (Table 4). The latter category, as defined in HANZE, represents short, rapid floods, where the extreme rainfall event triggering the event lasted no more than 24 hours, excluding urban floods. As those often occur in small catchments, they are often not captured as the study was limited only to catchments with an upstream area of at least 100 km^2.

The HANZE database indicates more than 6,000 NUTS3-level impacts since 1950. 78% of those are reproduced by the model (Table 4), a slightly higher percentage than the hit rate at event level (74%). This is largely due to good coverage for slow-onset riverine floods (88%) compared to flash floods (55%), when the former affected more regions on average than the latter. For the 1504 events matched by the model, the hit rate of NUTS3 regions for the model is 89%, again lower for flash floods (84%) than for larger riverine events (91%), not to mention coastal floods (98%). A full list of HANZE events with the information which of those were captured by the model, and which NUTS3 regions were correctly identified is provided together with the dataset on the repository (Paprotny, 2024). In general, performance of the model is stable over time (Fig. 6), though the share of events correctly identified by the model is lower in the very beginning of the model runs (1950s).

Analysing the reported impacts in HANZE, even though they are incomplete (except for fatalities), provides further insights. The data in Table 4 show that 97–100% of reported impacts in all four categories for coastal, compound and slow-onset riverine floods were in those historical floods that could also be found in the model. This shows that the model captured almost all large events, and the omissions are mostly minor floods in specific areas where the hazard is apparently not well quantified.

For instance, out of 14 omitted coastal and compound floods, 10 are events in Italy occurring mostly before 1964 and affecting 200–500 persons with no more than one fatality (with a single exception of a seven-fatality flood from January 1950). Much lower coverage is again for flash floods, as only those responsible for 61% of all fatalities can be found in the model. For other impact categories, the coverage is better, but historical records are very incomplete in relation to those statistics.

Table 4. Comparison of the number of HANZE events, their footprints and reported impacts, with modelled data, 1950–2020. * only regions classified as compound by the model – regions forming compound events in the HANZE database are not necessarily in the zone directly influenced by both riverine and coastal drivers; ** impact data is not available for all HANZE events.

Category	HANZE event type				All events
	Coastal	River/ Coastal	River	Flash	
Matching of events with impact data ("A" events)					
Number of events in HANZE database (1950–2020)	71	41	970	955	2037
Number of modelled events matched with HANZE	61	37	880	526	1504
Percentage of HANZE events matched with modelled events	90%	86%	91%	55%	74%
Matching of affected NUTS3 regions					
Number of affected NUTS3 regions in HANZE database	195	162	4058	1671	6086
Number of affected NUTS3 regions in matched HANZE events	180	152	3910	1084	5326
Number of regions that are also in the modelled events	177	97*	3553	915	4742
Percentage of all regions that are also in the modelled events	91%	60%*	88%	55%	78%
Percentage of matched regions that are also in the modelled events	98%	64%*	91%	84%	89%
Percentage of total reported impacts of all HANZE events within matched HANZE events (1950–2020) **					
Area inundated	99.8%	100%	99.5%	93.2%	99.2%
Fatalities	99.5%	99.4%	97.0%	61.2%	81.2%
Persons affected	99.3%	98.7%	98.9%	78.9%	96.3%
Economic losses in 2020 euros	99.8%	100%	98.9%	86.1%	96.1%
Matching of events without impact data ("B")					
Number of historical floods without impact data (list B)	27	12	119	79	237

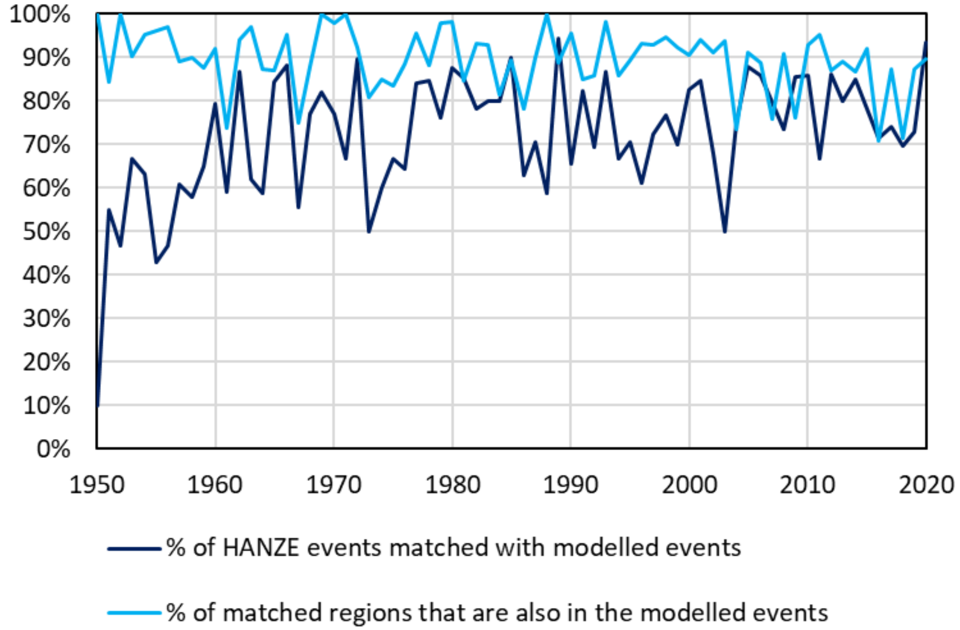

Figure 6. Share of HANZE events matched with the model, and the share of regions in matched events also present in the model.

3.2 Modelled potential impacts in the flood catalogue

Without flood protection measures, floods would have large consequences throughout Europe. A simple summation of flood impacts in the catalogue is not informative, as it assumes not only no flood protection, but also that population and economic activity move into the frequently affected zone in the first place, and then immediately return to previous conditions after each event, even just days after the previous. Considering the total reported impacts in HANZE v2.1, albeit incomplete, it can be estimated that only about 1% of potentially inundated area, population and economic assets were actually affected during 1950–2020. The reported flood deaths equal only about 0.01% of the potential fatalities. Therefore, the potential impacts are merely an intermediate result necessary in the process of estimating flood vulnerability and impact attribution (see section 5). Still, some analysis of the results can be performed as the modelling chain can derive the impact estimates under different exposure scenarios, and it was driven by variable climate conditions.

3.2.1 Temporal changes in potential flood impacts

For all types of events, an increase in the number of potential events and their impacts was recorded (Table 5). Even though the trends are less pronounced under constant exposure scenarios, they are still equivalent to at least 0.3% annual increase in potential coastal flood losses in an average year between 1950 and 2020 in case of fatalities, 0.5% in case of economic loss and 0.8% in case of affected population. For riverine floods, the potential impacts have grown even more, while the strongest increase is indicated for compound floods, at a rate of at least 1.9% per year since 1950. Potential impacts per flood event are rather similar for coastal and riverine events, and slightly lower for compound events, as the latter category is spatially constrained to regions directly affected by both coastal and riverine drivers.

Demographic and economic growth since 1950 has increased potential losses substantially. Presently, exposure of population to riverine floods is more than 50% higher than if population would have not increased, and nearly twice as high for coastal and compound events. Potential impacts relative to the total population in the study area increase more strongly than in the constant-exposure scenario, indicating stronger population growth in areas prone to coastal and compound flooding relative to areas not at risk. However, only a marginal increase in areas at risk of riverine floods was observed relative to areas not prone to this type of floods.

Enormous increase in gross domestic product (GDP) per capita (2% per year in the study area), and associated growth in the stock of fixed assets resulted in a five- to six-fold increase in potential losses relative to 1950, and eight- to ten-fold increase in 2020. As the asset growth was higher than GDP, potential economic losses relative to GDP also increased between 1950 and 2020. In contrast to population growth, asset growth in flood-prone areas was only marginally higher, or even lower in case of riverine events, than in areas not at risk of flooding.

Table 5. Average potential impacts of floods and their trends, by flood type and exposure scenario (dynamic year-of-event exposure, or fixed at 1950 or 2020 levels). The impacts of compound events mostly overlap with those of coastal and riverine, therefore they should not be added together. Economic losses in constant 2020 prices and exchange rates.

Flood type	Coastal			Riverine			Compound		
Exposure map	Dyna-mic	1950	2020	Dyna-mic	1950	2020	Dyna-mic	1950	2020
Average potential impacts per year									
Number of events	34	x	x	158	x	x	15	x	x
Area inundated (thsds. km^2)	27	x	x	182	x	x	13	x	x
Fatalities (thousands)	214	133	351	1,059	851	1,246	81	51	108
Persons affected (thousands)	2,689	1,966	3,590	15,284	11,919	18,247	1,004	704	1,239
Economic loss (billion euro)	237	50	478	1,200	261	2,196	86	14	149
Annual increase of potential impacts (%)									
Number of events	1.3	x	x	0.7	x	x	1.5	x	x
Area inundated	1.1	x	x	0.4	x	x	1.6	x	x
Fatalities	1.5	0.4	0.3	1.0	0.6	0.6	2.6	1.6	1.9
Persons affected	1.5	0.9	0.8	1.2	0.8	0.8	2.4	1.7	1.9
Economic loss	2.8	0.6	0.5	3.1	0.9	0.9	4.0	1.8	2.0
Increase in total impacts relative to 1950 exposure									
Fatalities	61%	x	164%	24%	x	46%	59%	x	111%
Persons affected	37%	x	83%	28%	x	53%	43%	x	76%
Economic loss	371%	x	852%	360%	x	742%	505%	x	948%

3.2.2 Spatial distribution of potential flood impacts

Coastal and compound flood potential is highly concentrated in just a few countries (Fig. 7). Though these estimates do not include the effect of flood protection, the top five countries by coastal flood potential are also most prominently featured in the HANZE database in terms of historical coastal flood impacts: the Netherlands, the United Kingdom, Germany, France, and Italy. The same group, plus Ireland, also have the most significant compound flood potential. On the other hand, numerous potential coastal and compound floods are present in the catalogue for Greece, but only one historical example for that country could be found in HANZE (a compound flood in 1968 that affected Crete).

In total, the flood catalogue includes coastal floods in 25 countries and compound floods in 24. Slovenia also has no event on the compound flood list, as none of the compound events was able to pass the higher socioeconomic thresholds for riverine and compound events. Bosnia and Herzegovina and Montenegro are the only countries on the compound flood list that are not present on the coastal flood list due to the limited risk along their short coastlines. Bulgaria is the only country with access to the sea that is not included in the coastal flood catalogue, as no event exceeded the socioeconomic thresholds. One historical case of coastal flooding in Bulgaria (in 1999) was recorded in HANZE.

Riverine flood potential is more evenly distributed in space. All countries highlighted in Fig. 7b have numerous examples of historical damaging floods in HANZE, with the exception of the Netherlands, where historical cases are limited to four floods recorded in the 1990s. In total, 37 out of 42 countries in the study area had at least some potential flood events. Some small countries had no riverine or compound floods in the catalogue, as they have no river section with an upstream area bigger than 100 km^2.

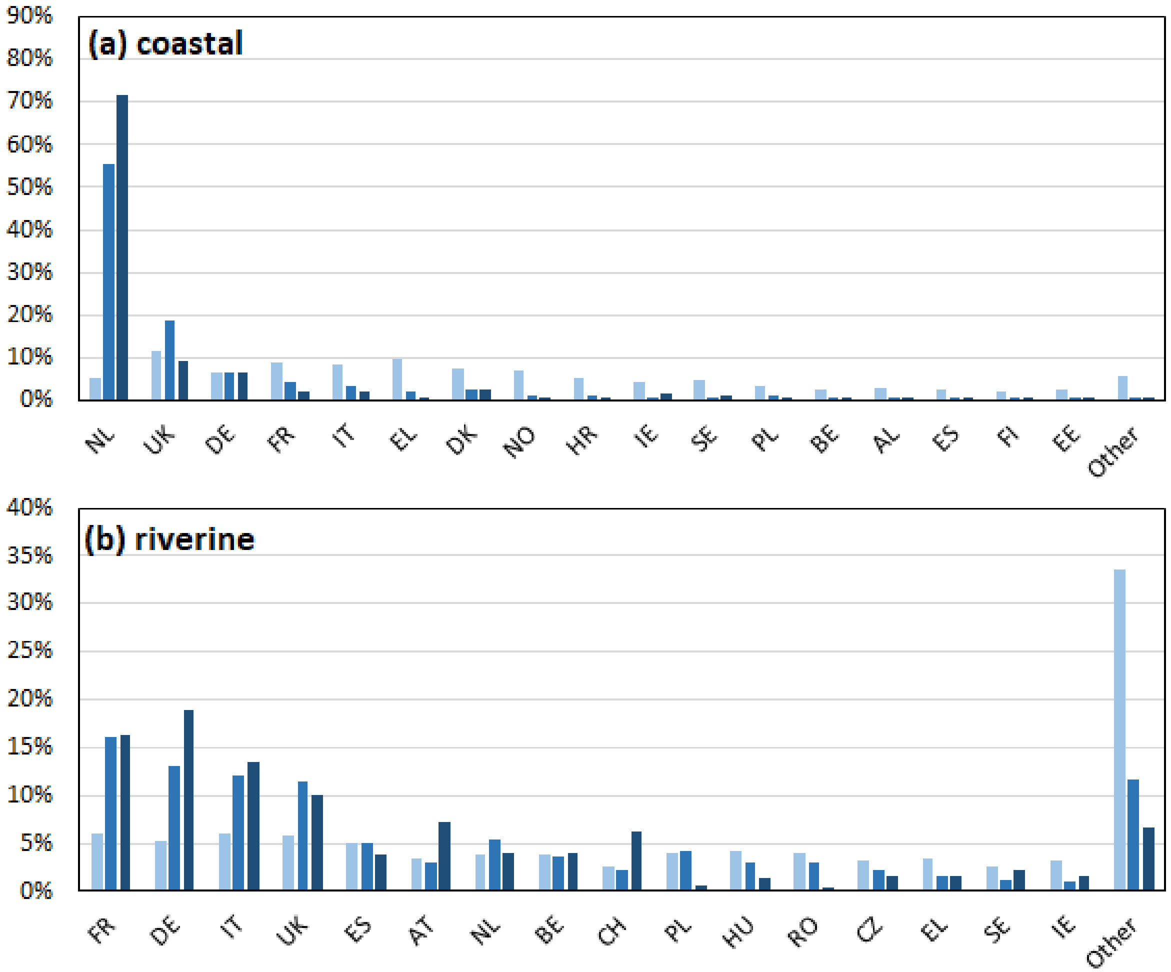

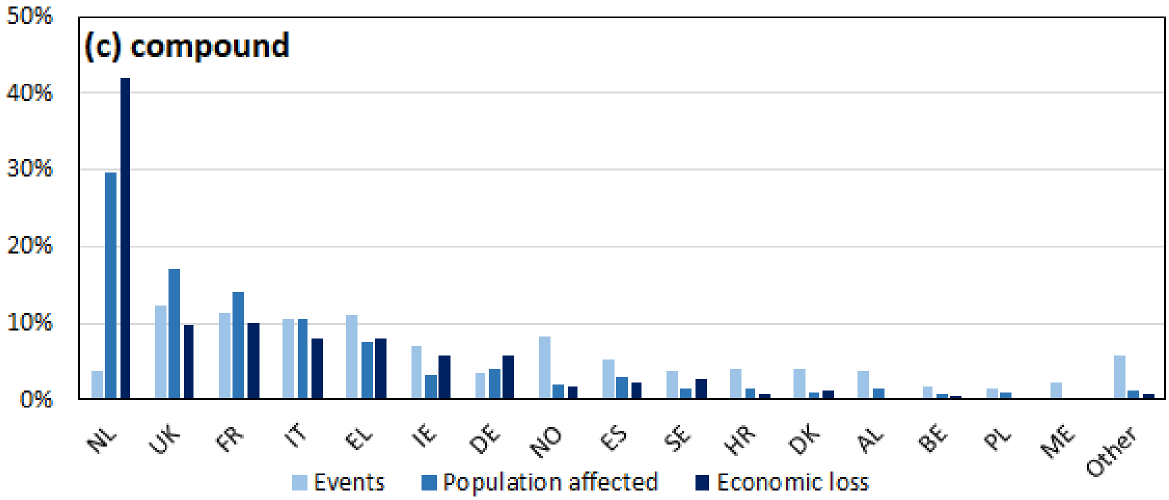

Figure 7. Flood events in the catalogue by country and potential impacts, as % of all events: (a) coastal, (b) riverine, and (c) compound. Population affected and economic loss in constant 2020 exposure.

A variety of indicators can be derived at the level of NUTS3 regions. Here we present one example, potential economic damages normalised to 2020 exposure level, relative to 2020 gross domestic product (GDP). Along most of the European coast potential damages resulting from storm surges are limited (Fig. 8), with risk concentrated along the North Sea, Adriatic Sea, and Aegean Sea. Locations of the most significant past coastal floods stand out (the Netherlands, German Bight, Venice). Riverine damage potential is much higher (Fig. 9), and concentrated around main European mountain ranges (Alps, Carpathians, Pyrenees, Dinaric Alps), as well as Scandinavia and British Isles. Risk is noticeably lower along the Northern European Plain, southwestern Iberian Peninsula, and southern Great Britain. However, it must be stressed that the data represent only damage potential, without considering flood protection or other forms of adaptation.

In some parts of Europe, the possibility of co-occurrence of coastal and riverine floods could have large implications on risk. Fig. 10 maps the share of compound flood potential at regional level relative to the total. For each NUTS3 region, we derived a list of all flood events with a potential inundated area of 100 ha, i.e. before aggregation and application of socioeconomic thresholds, then removed riverine and coastal events that overlapped with compound events. In this way, it was possible to avoid double counting and sum together the remaining flood events. The results (Fig. 10) show that compound potential is very unevenly distributed across Europe. In northern and eastern coasts of the Adriatic Sea, Greece, Ireland, western and southern coasts of Great Britain, and certain parts of France, Italy, Spain, and Norway, compound events could potentially contribute 20–25% or even more of all economic losses from flooding. In all aforementioned countries there are known examples of damaging floods contained in the HANZE database.

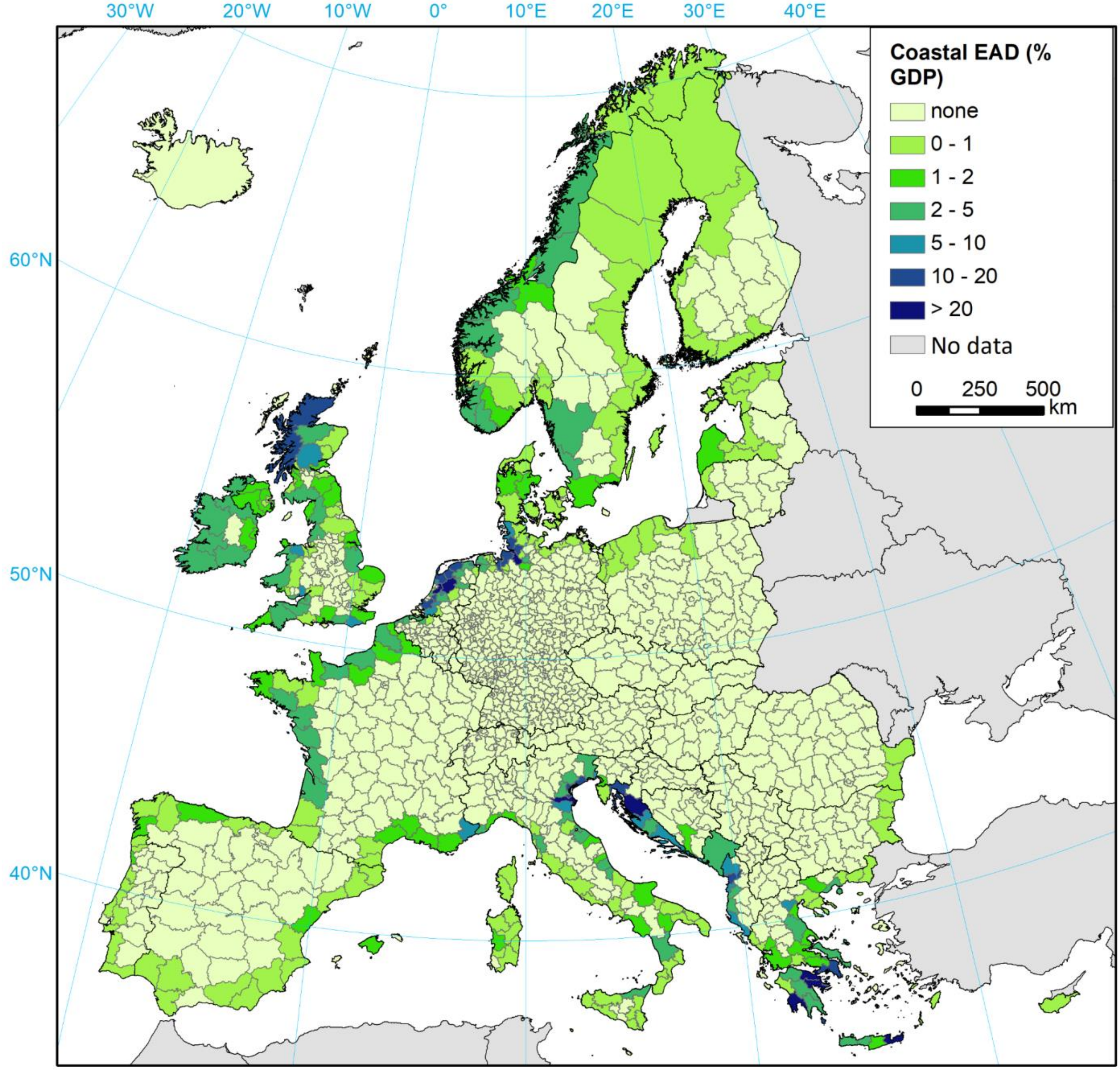

Figure 8. Potential expected annual economic damage of coastal floods as % of GDP, 1950–2020, in constant 2020 exposure, per NUTS3 region. Potential impacts per region include all events above 100 ha flooded area threshold per NUTS3 region, including those not passing the socioeconomic impact thresholds.

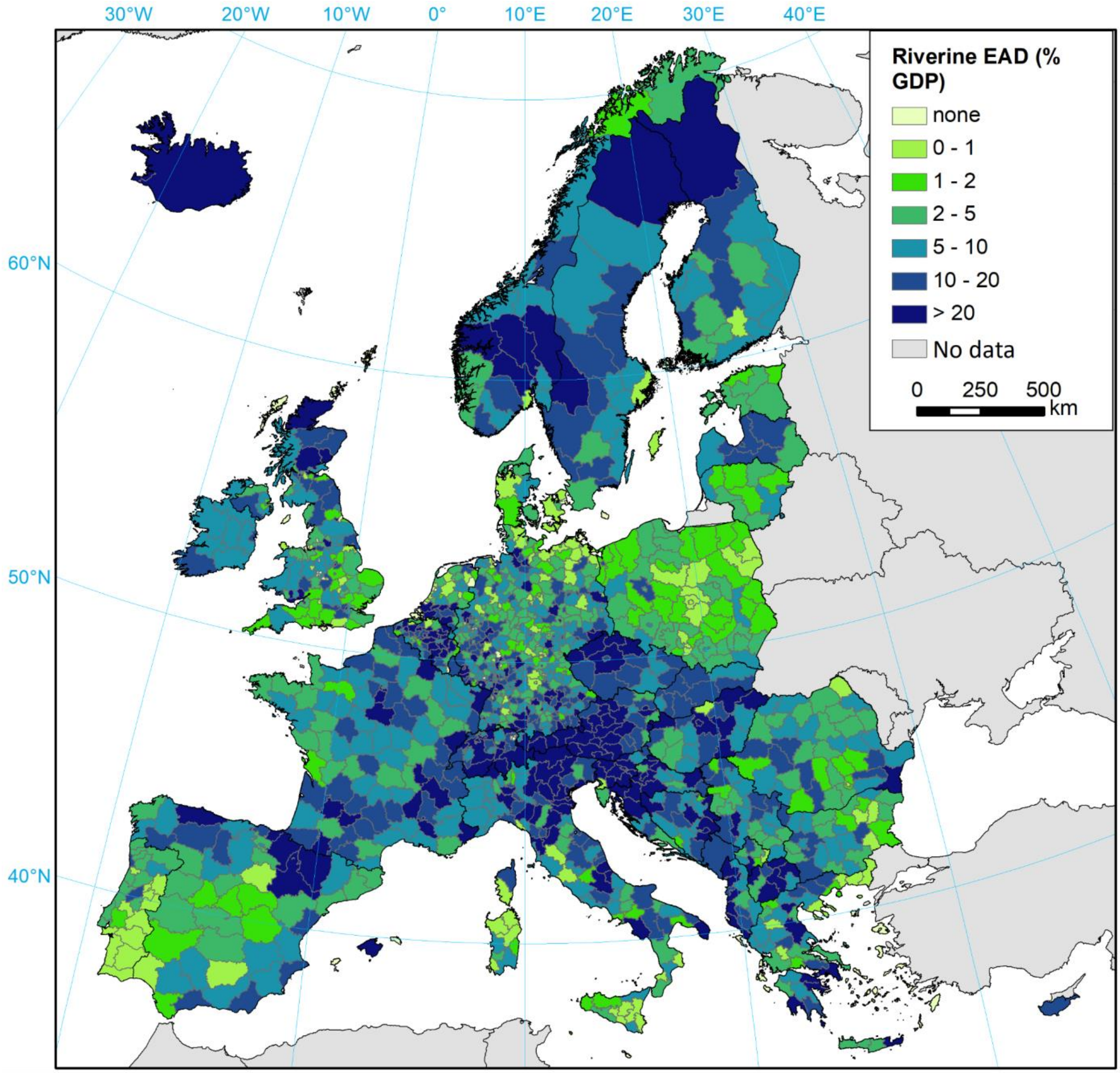

Figure 9. Potential expected annual economic damage of riverine floods as % of GDP, 1950–2020, in constant 2020 exposure, per NUTS3 region. Potential impacts per region include all events above 100 ha flooded area threshold per NUTS3 region, including those not passing the socioeconomic impact thresholds.

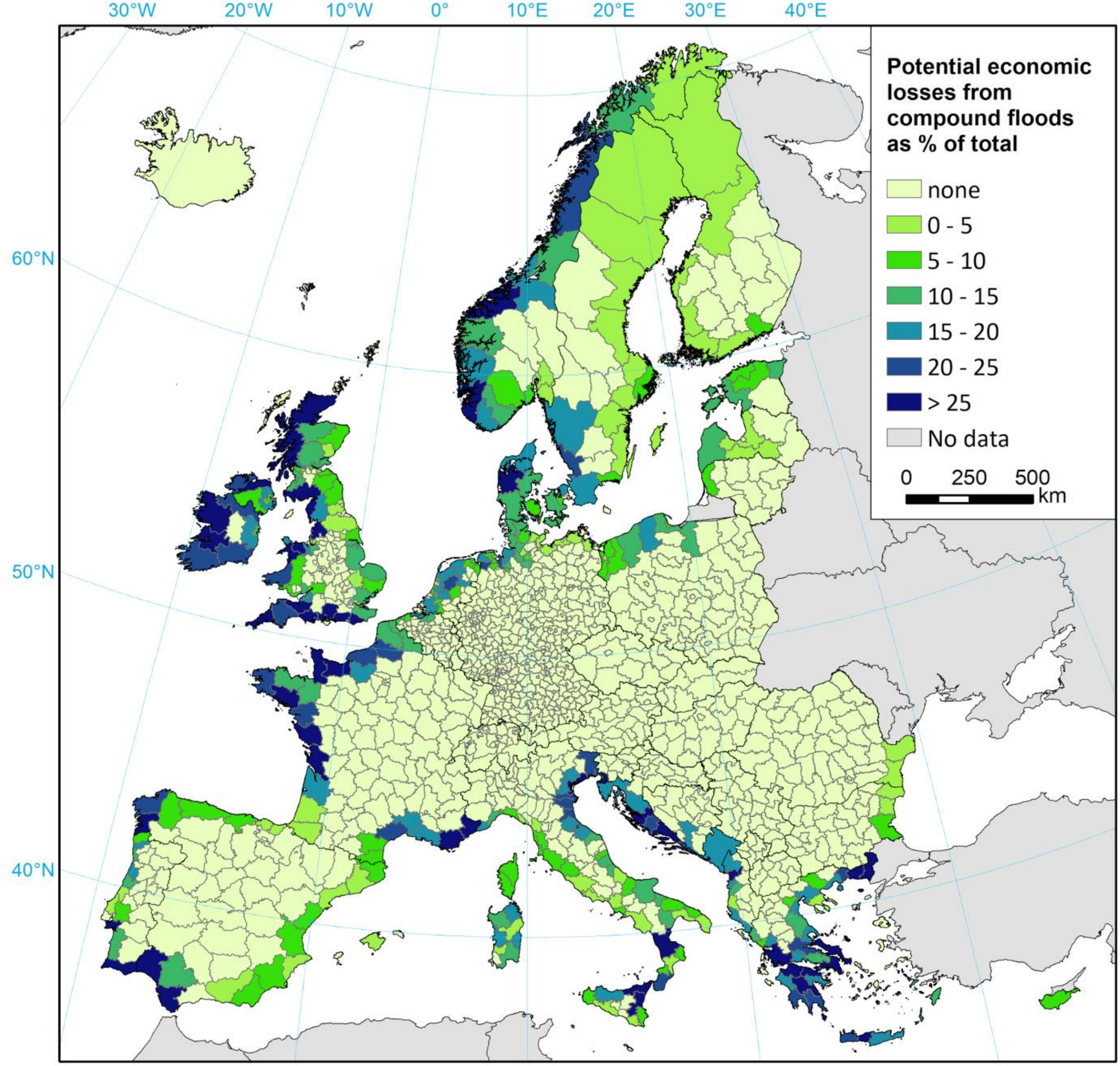

Figure 10. Share of compound floods is total potential economic losses, 1950–2020, in constant 2020 exposure, per NUTS3 region. Potential impacts per region include all events above 100 ha flooded area threshold per NUTS3 region, including those not passing the socioeconomic impact thresholds. Individual riverine and coastal events contributing to compound events were excluded to compute this metric.

3.3 Validation

3.3.1 Extreme river discharges

At least one river discharge station with adequate data length was available for 7742 events (63% of the total), and nearly 292,000 timeseries were identified within the NUTS3 regions potentially affected by those events. Most of the data is available for events that have occurred in the United Kingdom, Poland, Spain, Sweden, Germany, France, and Norway. The R^2 between modelled and observed peak discharge for all event time series, standardised by reported upstream area, is 0.45. However, the relative discharges are more of interest of this study, and modelled peak discharges corrected for difference in average annual discharges have an R^2 of 0.63. The timeseries of daily discharge during the events is good (0.5-0.75) or very good (0.75-1) for 59% of all station-events in terms of Spearman's R^2, and for 30% in terms of KGE score. On the other hand, poor (0-0.2) or very poor (<0) performance was recorded for 18% and 41% of stations, respectively. There is relatively little difference in performance depending on classification of events, except for far worse results for events classified as false positives ("E"). Here, the poor or very poor score was recorded for 83% of station-events, compared to 37% for HANZE flood events ("A"). Performance also varies strongly by location (Fig. 11), with e.g. Germany, Ireland, Austria, Belgium, and Slovakia recording much higher shares of good or very good station performance (above 40%) than e.g. Poland, Spain, Sweden, and Portugal (less than 25%).

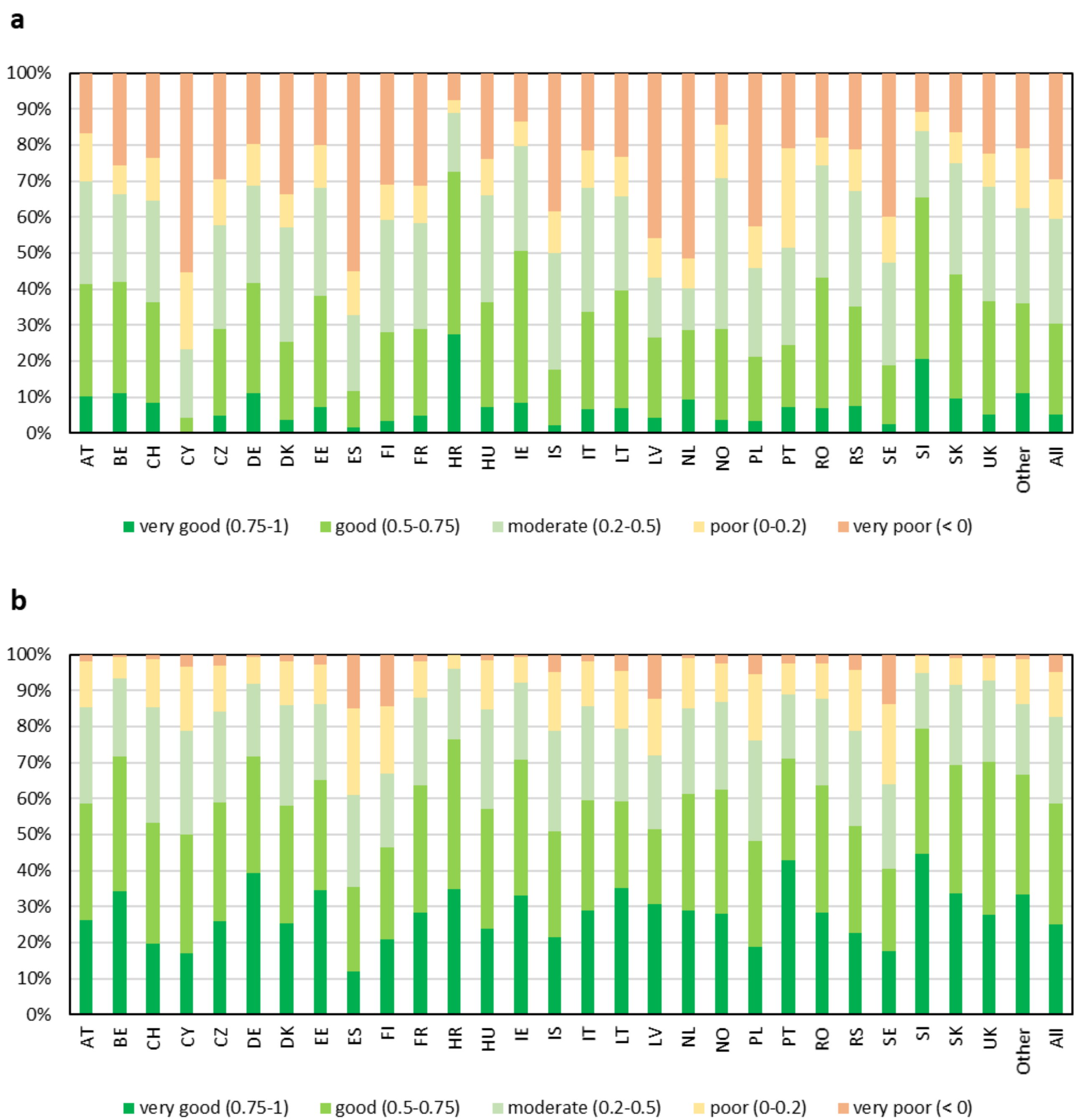

Figure 11. Comparison of daily river discharge during flood events in the catalogue, or a 30-day window centred around the dates of the event. Abbreviations are NUTS level 0 country codes. The graph shows the percentage of all stations per country by performance class: (a) KGE score; (b) Spearman's coefficient of determination.

3.3.2 Extreme sea levels

At least one tide gauge with adequate data length was available for 1363 events (56% of the total), and a total of 8102 time series were identified within the NUTS3 regions potentially affected by those events. Most of the data is available for events that have occurred in the United Kingdom, Denmark, Norway, the Netherlands, France, Sweden, and Germany. The overall results are compared using several metrics in Table 6. Overall, the maximum sea levels observed during the various potential coastal floods were well reproduced, with the main source of inaccuracies being storm surge heights. Further, 80% of modelled time series spanning the duration of the events indicated a good or very good R^2 when compared with observations. For tides and total water level, such performance was measured for 93–94% of stations. The best performance of the storm surge model was recorded for North and Baltic seas (Fig. 12), with far lower performance for the Eastern Mediterranean Sea. However, potential flood events and observational data are both relatively scarce in the latter region, which had the lowest scores also for reproducing tides and combined sea level. As in the case of riverine events, there is little variation between events by classification, though historical HANZE events ("A") had slightly higher scores for storm surge heights and combined sea level than all other classes. This could be, to some extent, the result of the difference in the geographical distribution of events.

Table 6. Comparison between maximum hourly sea level and its components during flood events in the catalogue, or a 7-day window centred around the dates of the event.

Metric	Storm surge height	Tide elevation	Combined sea level
Pearson's R^2	0.75	0.99	0.96
Spearman's R^2	0.74	0.95	0.94
Nash-Sutcliffe Efficiency	0.47	0.99	0.96
Root mean squared error (RMSE) in metres	0.30	0.14	0.26
RMSE to standard deviation ratio	0.53	0.11	0.21

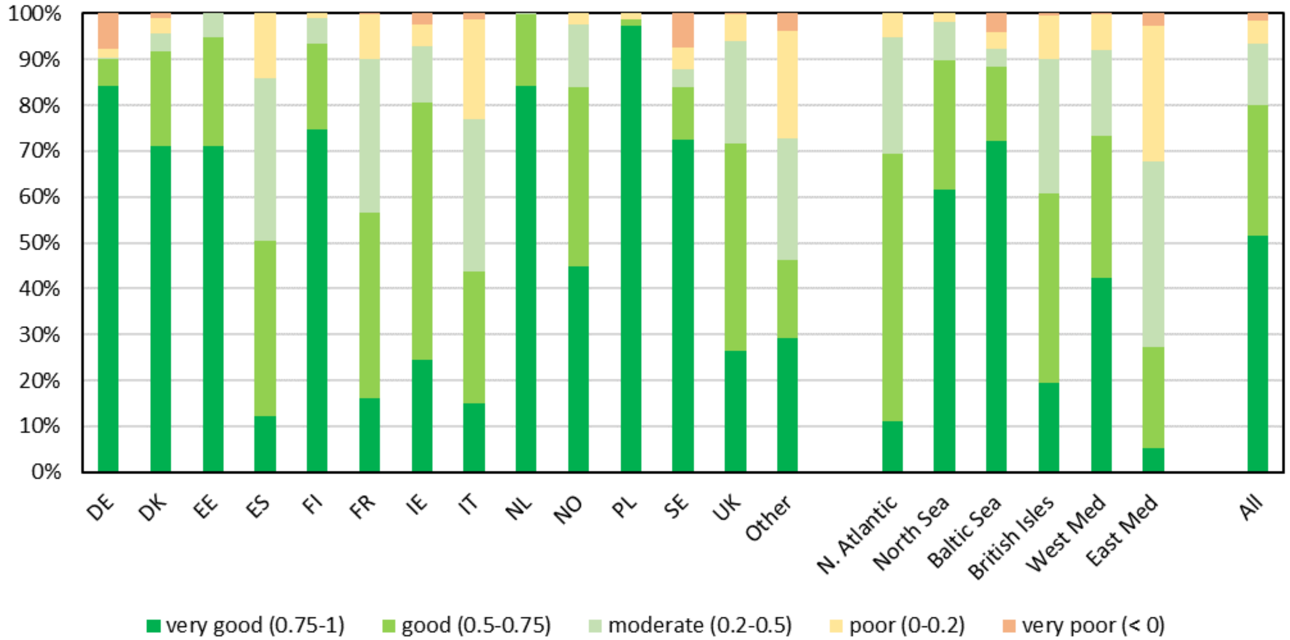

Figure 12. Comparison between maximum hourly storm surge height during flood events in the catalogue, or a 7-day window centred around the dates of the event. The graph shows the percentage of all stations per country by performance of Pearson's R^2. Abbreviations in the left side of the graph are NUTS level 0 country codes. On the right side of the graph, stations are grouped by main European sea regions: "N. Atlantic" – exposed North Atlantic Ocean coasts (mostly France and Spain), "North Sea" – including Norwegian coasts, "Baltic Sea" – including Danish Straits, "British Isles" – coasts of Great Britain and Ireland, "West Med" and "East Med" – Western and Eastern Mediterranean Sea, respectively.

3.3.3 Comparison of flood footprints

Comparison of modelled potential flood impacts with impacts based on satellite-derived flood footprints and actual impacts recorded in the HANZE database highlights the challenge of correctly recreating past floods (Table 7). For exactly half of the 20 floods for which a satellite-derived footprint is available, our modelled population affected were closer to reported population affected than estimates based on satellite-derived flood footprints, and vice versa. In most cases, satellite-derived footprints severely underestimated the extent of the flooding, with the exception of floods in the United Kingdom, where they indicated many times more affected population than the reported actual impact. In all cases the modelled area and persons affected were higher than the actual impact, as was the intention of the catalogue, as modelled without flood protection. However, there is a very close match in persons affected during the August 2002 flood in Czechia and Germany. In the whole catalogue, the area affected was higher than reported in 83% of cases where the actual impact was reported in HANZE (i.e. 256 out of 307), fatalities in 98% of cases (1473 out of 1496), population affected in 89% of cases (686 out of 773) and economic loss in 89% of cases (675 out of 755).

Table 7. Comparison of modelled potential flood zone with satellite-derived footprints from the Global Flood Database (Tellman et al., 2021) and reported impacts from HANZE (Paprotny et al., 2023) for several European floods, 2002–2015. Area flooded in km^2. * percentage of the satellite flood footprint reproduced by the modelled flood footprint of this study.

Event (country, month, year)	**HANZE ID**	**Reported impacts (HANZE)**		**Modelled impacts with potential flood zone**		**Modelled impacts with satellite footprints**		**Hit rate modelled area to satellite area***	**Ratio of affected population**	
		Area flooded	Persons affected	Area flooded	Persons affected	Area flooded	Persons affected		Modelled: reported	Reported: satellite
Albania, November/ December 2010	2031	139	24,700	894	91,776	194	8,260	56%	3.7	3.0
Austria, March 2006	21		1,840	263	15,130	68	1,659	45%	8.2	1.1
Bosnia and Herzegovina, April-May 2004	2053	200	20,000	734	147,114	75	1,023	44%	7.4	19.6
Czechia, August 2002	86		225,000	1247	225,513	90	4,018	54%	1.0	56.0
France, September 2002	244		12,000	763	116,813	95	1,595	30%	9.7	7.5
France, December 2003	250		27,000	1,843	245,870	767	11,954	67%	9.1	2.3
Germany, August 2002	341		330,000	3,371	372,649	681	10,081	74%	1.1	32.7
Greece, January/ February 2015	403	250	500	405	3,696	268	256	44%	7.4	2.0
Hungary, March-May 2006	421	2,440	5,400	5,201	310,750	918	10,886	37%	57.5	0.5
Hungary, May/June 2010	422	1,230	5,000	1,376	77,306	199	214	85%	15.5	23.3
Italy, November/ December 2002	952		10,000	2,031	424,594	119	29,321	13%	42.5	2.9
Italy, January 2003	954		40,000	370	43,917	35	392	18%	1.1	102.0
Lithuania, March/April 2010	2200	400	2,000	1,211	27,851	214	464	59%	13.9	4.3
Montenegro, December 2010	2209		6,630	289	21,390	198	2,330	34%	3.2	2.8
Poland, May/June 2010	1065	5,540	280,000	7,151	775,536	348	9,757	71%	2.8	28.7
Romania, July 2005	1148	993	58,700	1,664	85,918	338	1,061	50%	1.5	55.3
Romania, April/May 2006	1153	1,165	15,011	5,305	115,330	3,415	6,626	43%	7.7	2.3
UK, November/ December 2012	1558		4,400	1,156	132,320	869	265,903	12%	30.1	0.02
UK, December 2013-February 2014	1561	450	25,000	828	225,781	815	388,930	13%	9.0	0.06
UK, December 2015-January 2016	1563		64,000	1,016	100,633	1,472	480,026	9%	1.6	0.13

Direct comparison between modelled and satellite footprints (Fig. 13) has shown that the hit rate, i.e. share of the satellite footprints correctly reproduced by the model, varied between 30 and 85%, except for events in Italy and the United Kingdom, where it was only 9–18%. However, the satellite footprints also performed very poorly against reported losses for those floods. Some additional flood events were analysed, but were not included in Table 7 as the satellite footprints showed virtually no population affected, which is in large contrast to actual impacts. Such a situation occurred e.g. for the summer floods in the United Kingdom in 2007 that flooded homes of about 192,000 people (HANZE database number 1546), almost none of which could be reproduced with satellite flood footprints.

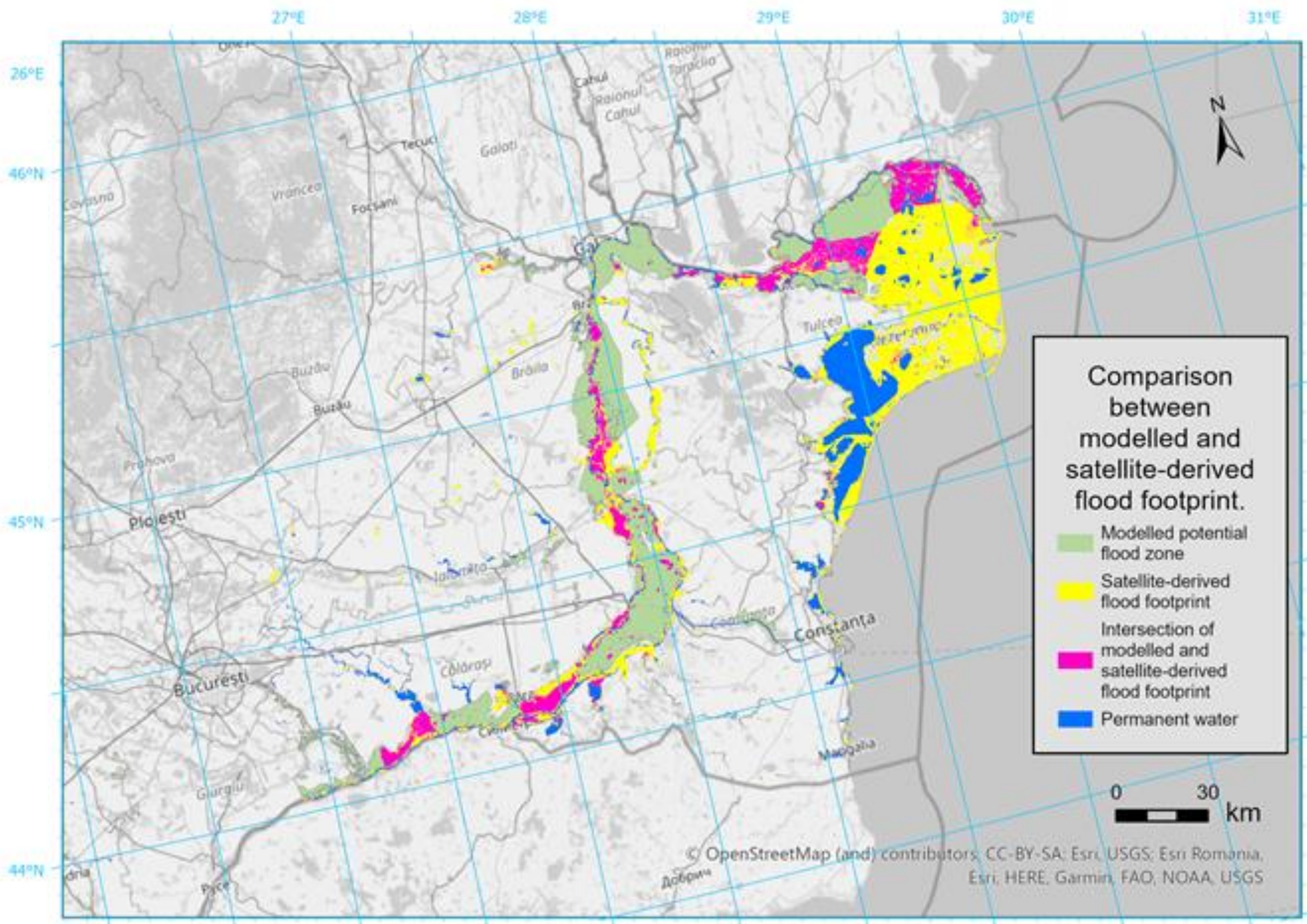

Figure 13. Example comparison between modelled and satellite-derived flood footprint of the 2006 event in Romania.

4 Discussion

4.1 Uncertainties and limitations of the models and modelled data

The elaborate modelling chain involving both riverine and coastal processes is subject to multiple cascading limitations and uncertainties. The starting point of the simulations are input climate data, derived from global reanalyses. Though ERA5 and

ERA5-Land are state-of-the-art, they still encounter problems of inhomogeneities, gaps or errors in observational data, model biases, and limitations in representing precipitation extremes in particular (Hersbach et al., 2020, Muñoz-Sabater et al., 2021). In the case of the riverine model, bias-adjustment and downscaling was carried out, but it is also only a statistical transformation that depends on the quality of high-resolution observations as well (see section 4.1.2).

Validation results in section 3.1 indicate mostly good performance of the models in reconstructing past extreme discharges and sea levels, but not in all areas. Some regions are more challenging to model than others, e.g. due to complex topography or shoreline, or strong anthropogenic influence on the water cycle (especially through reservoirs). Not all types of floods or processes that drive them could be represented. Most noticeably, the resolution of the riverine model is inadequate to capture smaller flash floods, as the hydrological model has a spatial resolution of 1' driven by climate data that was twice downscaled (first from ERA5 to ERA5-Land, then using ISIMIP3BASD method) and with a temporal resolution of six hours. Additionally, flood hazard maps used to generate the footprints only covered catchments with an upstream area of at least 100 km^2. Consequently, 91% of slow-onset riverine floods from HANZE were reproduced, but only 55% of flash floods. Urban floods are not represented at all (also in the HANZE dataset).

Further, no flood defences are represented in the model, which is by design, as information on this aspect is scarce, especially in the temporal dimension. At the same time, a flood that was historically prevented by existing defences might not have been prevented under counterfactual conditions. We also hypothesise that flood protection levels are driven to some extent by flood risk and flood occurrence (section 4.2). The use of flood hazard maps for a defined set of scenarios enables generating flood footprints without carrying out a computationally infeasible continuous hydrodynamic simulation over a period of 71 years. However, the maps assume a specific hydrograph which is not necessarily valid for all floods with the same peak discharge. Further, the three sets of maps (including two sets for different catchment sizes) are methodologically different and were created for diverse sets of scenarios. Whereas the coastal maps were rerun specifically for this study based on the results of the extreme sea level modelling, the riverine maps are from previous studies. Their application is in some locations problematic due to inconsistencies in river network delineation between EFAS and the hazard maps. The accuracy of the riverine flood hazard maps is also variable depending on the region and the probability of occurrence (see Paprotny et al., 2017, and Dottori et al., 2022, for details).

Compound floods are represented by merging riverine and coastal flood zones, which neglects the possible interaction between the storm surge and river discharge that could generate higher water levels than is possible for individual drivers. Additionally, not all coastal processes are included in the model, such as interaction between tide and storm surges, or influence of SLR on tide elevations. Wave run-up is only approximated by taking one-fifth of offshore significant wave height, as more precise estimates would require a very detailed model of the nearshore. Finally, long-term land motion is limited to GIA due to lack of detailed data on the subject.

4.2 Uncertainties and limitations of the observations and documentary sources

The results are influenced not only by the accuracy of models, but also that of the observations. Our river discharge simulations are driven by reanalysis data that were downscaled and bias-adjusted using interpolated meteorological observations, the accuracy of which depends strongly on the density of point meteorological data. As shown in Thiemig et al. (2022), precipitation during extreme events in the EMO dataset can at times diverge strongly from other reported measurements. Though our meteorological input data is still driven primarily by ERA5, the reanalysis itself is influenced by availability of meteorological data, which is very inhomogeneous in time (Hersbach et al., 2020). This might be the reason for the noticeably lower performance of our model in reproducing flood events in the 1950s.

Model calibration and validation, as well as classification of the flood event catalogue is affected by the availability of tide and river gauges (section 3.1.1 and 3.1.2). The data is unevenly distributed, with most data available for northern Europe, particularly the Nordic countries and the British Isles. On the other hand, very limited data was available for Italy, Greece, and Balkan countries. It is further uneven in time, with both the 1950s and the last few years until 2020 having lower coverage than the 1990s and 2000s in particular. Identification of events as false positives ("E") is also potentially problematic, as in large NUTS3 regions the only available observations could be outside the impact zone of the event, hence incorrectly suggesting that the model generated a 'bogus' event. Satellite-derived footprints were used to compare the modelled flood footprints, but themselves often widely diverged from reported impacts. The hit rate between satellite and model data varied significantly between individual events, similarly observed in a reconstruction of recent European coastal floods by Le Gal et al. (2023).

Similarly, documentary sources on socioeconomic impacts of floods are highly uneven in quality between countries. For instance, while there are comprehensive databases and flood catalogues accessible e.g. for France, Italy, Norway, Portugal, Spain, or Switzerland, and even some Balkan countries, scattering of information makes it very laborious to collect data for other countries, e.g. Austria, Germany, and the United Kingdom. Many compilations of flood impacts only cover the recent two decades, while older flood catalogues published in the 1980s or 1990s often have no newer follow-ups. This strongly affects the frequency of "C" (No impacts) events relative to "D" (Impacts unknown). Thanks to extensive research in the HANZE database, this has less effect on detection of "A" (Impacts, data) and "B" (Impacts, no data) events. Still, uncertainty surrounds designation of flood events as having "significant" socioeconomic impacts. The thresholds defined in HANZE are somewhat arbitrary, though based on experience of collecting more than 2500 records in the dataset. In case of smaller events, their classification is uncertain if the data is incomplete or not very accurate. This is potentially problematic for "B" events, where at times no quantitative data at all is available, and the classification was based on the description of impacts only. Finally, NUTS3 regions, the principal socioeconomic unit of observation here and in HANZE, vary in size both in terms of area and population. It might be slightly easier for floods in large regions to pass region-scale threshold for minimum flood area in the model, and to be considered affected in HANZE, where region-scale impact thresholds are also applied when detailed damage data are available.

5 Conclusions

This study is the largest attempt to reconstruct past flood losses in Europe, and makes an advance towards full decomposition of drivers of historical flood losses. We created a flood catalogue for Europe containing 14,699 events with significant socioeconomic impact potential. It covers riverine, coastal and compound events over a period of 71 years, and considers climate change, evolving human impact on catchments, and growing exposure. However, it should be highlighted that the damage estimates provided in the catalogue exclude the influence of flood defences, and spatial and temporal variation of vulnerability levels.

The catalogue includes 1504 out of 2037 damaging floods since 1950 included in HANZE dataset (Paprotny et al., 2023), including some 90% of coastal, compound and slow-onset riverine floods, and 55% of flash floods. The coverage of reported impacts of those events is 81-99% depending on the exact measure. The performance of the model is relatively stable over time, though slightly worse for the 1950s.

The flood catalogue was primarily devised as the baseline (factual) reconstruction of past floods in Europe. However, it can be also used directly for multiple applications. The immediate follow-up to this analysis will be modelling changes in flood preparedness in Europe in the past 70 years, including flood protection standards and relative losses (Paprotny et al., 2024). The modelling chain can be further used with counterfactual climate inputs. Methods such as ATTRICI (Mengel et al., 2021) enable removing the global warming effect from all variables required to model riverine discharges. Additional counterfactual simulations are possible to quantify the human influence on catchments, particularly through construction of reservoirs (Boulange et al., 2021). Methods such as transformed-stationary extreme value analysis (Mentaschi et al., 2016) can be used to detrend storm surge heights in addition to removing the long-term sea level rise. Together with HANZE historical exposure maps (Paprotny and Mengel, 2023), counterfactual scenarios for all components of risk would be achieved. This would provide the first comprehensive impact attribution of European flood losses and generate an important reference dataset for pan-European flood risk assessments.

Data availability: Numerous public datasets and models were used in the study, results of which are also publicly available. Details were to find each dataset and model are provided in Appendix A3. The flood event catalogue is also accessible through https://naturalhazards.eu/.

Code availability: The main code for generating the flood catalogue is available from Zenodo (https://doi.org/10.5281/zenodo.10678820). More links to other models and code are provided in Appendix A3.

Author contributions. DP developed the concept, implemented the methods, collected and processed most of the data, and acquired funding. BR collected part of the historical impact data and performed part of the flood event classification. MV computed coastal flood hazard maps. PT and JS performed the comparison based on satellite-derived flood footprints and created the online visualisation of the study. FD and ST contributed datasets and methods for the riverine and coastal simulations, respectively. LF and HK helped to develop the concept and methods. All authors wrote the paper.

Competing interests. The authors declare that they have no conflict of interest.

Financial support. This research has been supported by the German Research Foundation (DFG) through project "Decomposition of flood losses by environmental and economic drivers" (FloodDrivers), grant no. 449175973.

Appendix A1. Contents of "B" list of historical floods

The format of the database of "B" list events follows the same format of HANZE database (Paprotny et al., 2023), with a reduced number of fields as events were confined to the "B" list specifically due to lack of relevant data (primarily flood impact statistics). Most fields have strictly-defined permitted values, except "Notes", which includes explanation why impacts should be considered significant (using partial available data or descriptive indicators), and "Data sources" which lists all cited references. The latter are often the same as used in the HANZE database, therefore only publications specific to the B list are included in the full bibliographic details provided with the event file. For detailed discussion about the contents of each field we refer to Paprotny et al. (2023).

Table A1. Summary of fields recorded in the "B" list of floods.

Variable	Short description	Field type	Permitted values
ID	Unique event identifier	integer	7000…8999
Country code	Two-letter country code	string	Codes from Table B1
Year	Year of the event	integer	1950…2020
Country name	Country name	string	Names from Table B1
Start date	Daily start date	date	1.1.1950…31.12.2020
End date	Daily end date	date	1.1.1950…31.01.2021
Type	Detailed type of event	string	River, Flash, Coastal, River/Coastal
Regions affected (NUTS3 v2010)	Regions were human or economic losses were reported, at NUTS3 level (version 2010)	string	Codes from Table B2
Regions affected (NUTS3 v2021)	As above, but at using NUTS version 2021	string	Codes from Table B3
Notes	Other relevant information or notes on issues with the data	string	Free text
References	List of publications and databases from which the information was obtained	string	Free text

Appendix A2. Contents of the modelled flood event catalogue

Table A2. Summary of fields recorded in the modelled flood event catalogue.

Variable	Short description
ID	Unique event identifier
Country code	Two-letter country code
Year	Year of the event
Country name	Country name
Start date	Daily start date
End date	Daily end date
Type	Detailed type of event
Flood source	Rivers or sea basins in the potentially-affected area (from Vogt et al., 2007, and Fourcy and Lorvelec, 2013)
Regions affected (NUTS3 v2010)	Regions were human or economic losses were reported, at NUTS3 level (version 2010)
Regions affected (NUTS3 v2021)	As above, but at using NUTS version 2021
Area inundated	Potential inundated area in hectares (ha)
Fatalities, YE	Potential fatalities, in persons, year-of-event exposure
Fatalities, 1950	Potential fatalities, in persons, 1950 exposure
Fatalities, 2020	Potential fatalities, in persons, 2020 exposure
Persons affected, YE	Potential persons affected, in persons, year-of-event exposure
Persons affected, 1950	Potential persons affected, in persons, 1950 exposure
Persons affected, 2020	Potential persons affected, in persons, 2020 exposure
Economic loss, YE	Potential direct economic loss, in thousands of 2020 euros, year-of-event exposure
Economic loss, 1950	Potential direct economic loss, in thousands of 2020 euros, 1950 exposure
Economic loss, 2020	Potential direct economic loss, in thousands of 2020 euros, 2020 exposure
Loss threshold	Threshold for direct economic losses applied to the event, in thousands of 2020 euros
Mean water depth	Average water depth in the potential inundated zone
Return period	Average (geometric) of return periods along potential affected river grid cells or coastal segments, from detrended 1950–2020 data, Generalised Pareto distribution
Hydro data	Indicates if river or tide gauge data were available for this event (1 – yes, 0 – no)
RP2 exceedance	Indicates if a 2-year return period was exceeded in the observational data (1 – yes, 0 – no)
Category	Classification of event according to Table 3
HANZE ID	Flood event ID if event classified as “A” or “B”, otherwise empty field

Appendix A3. Availability of data and models

Table A3. Availability of input and output data and models from the study. Models are indicated by *italics*.

Variable, data	Dataset/*model*	Resource link
River discharges	HERA	https://data.jrc.ec.europa.eu/dataset/a605a675-9444-4017-8b34-d66be5b18c95
Meteorological data for storm surge simulation, significant wave height	ERA5	https://doi.org/10.24381/cds.e2161bac
Hydrodynamic model (coastal)	*Delft3D*	https://oss.deltares.nl/web/delft3d/get-started
Tide elevation constituents	FES2014	https://www.aviso.altimetry.fr/en/data/products/auxiliary-products/global-tide-fes.html
Tide elevation model	*pyTMD*	https://github.com/tsutterley/pyTMD
Mean dynamic topography	Global Ocean Mean Dynamic Topography	https://doi.org/10.48670/moi-00150
Sea level rise	Hourly Coastal water levels with Counterfactual	https://zenodo.org/records/7771386
Sea level rise	European Seas Gridded L 4 Sea Surface Heights	https://doi.org/10.48670/moi-00141
Sea level rise	Global Ocean Gridded L 4 Sea Surface Heights	https://doi.org/10.48670/moi-00148
Glacial isostatic adjustment	ICE-6G_C	https://www.atmosp.physics.utoronto.ca/~peltier/data.php
Storm surge heights, combined water level, tide levels	This study	https://doi.org/10.5281/zenodo.10630338
DEM for coastal inundation	GLO-30	https://doi.org/10.5069/G9028PQB
Hydrodynamic model for coastal inundation	*Lisflood-ACC*	*https://www.seamlesswave.com/LISFLOOD8.0*
Land use and population at 100 m resolution	HANZE v2.0 output maps	https://doi.org/10.5281/zenodo.7885990
Exposure model (population, fixed assets by sector)	*HANZE v2.0*	https://doi.org/10.5281/zenodo.7556953
Historical flood impacts ("A" list) and list of references	HANZE v2.1	https://doi.org/10.5281/zenodo.11259233
Significant flood events without direct impact data ("B" list)	This study	https://doi.org/10.5281/zenodo.10949631
List of documentary sources used	This study	https://doi.org/10.5281/zenodo.10949631
Coastal flood hazard maps, flood catalogue input data	This study	https://doi.org/10.5281/zenodo.10630862
River flood hazard maps	JRC maps	https://doi.org/10.2905/1D128B6C-A4EE-4858-9E34-6210707F3C81
River flood hazard maps	RAIN project maps	https://doi.org/10.4121/uuid:968098ce-afe1-4b21-a509-dedaf9bf4bd5
Historical flood database	EM-DAT	https://public.emdat.be/
Historical flood database	EEA Flood Phenomena	https://www.eea.europa.eu/data-and-maps/data/european-past-floods/flood-phenomena
Historical flood database	Dartmouth Flood Observatory	http://floodobservatory.colorado.edu/Archives/index.html
Historical flood database	FFEM-DB	https://doi.org/10.4121/14754999.v2
Historical flood database	Recorded Flood Outlines	https://www.data.gov.uk/dataset/16e32c53-35a6-4d54-a111-ca09031eaaaf/recorded-flood-outlines
River discharge data	GRDC	https://portal.grdc.bafg.de/
River discharge data (France)	HydroPortail	https://www.hydro.eaufrance.fr/rechercher/entites-hydrometriques

River discharge data (Norway)	NVE, Historiske vannføringsdata til produksjonsplanlegging	https://www.nve.no/vann-og-vassdrag/hydrologiske-data/historiske-data/historiske-vannfoeringsdata-til-produksjonsplanlegging/
River discharge data (Spain)	Centro de Estudios Hidrográficos, Anuario de aforos	https://ceh.cedex.es/anuarioaforos/default.asp
River discharge data (Sweden)	SMHI Vattenweb	https://www.smhi.se/data/hydrologi/vattenwebb
River discharge data (UK)	UK National River Flow Archive	https://nrfa.ceh.ac.uk/
River discharge, sea level data (Poland)	IMGW-PIB, Dane Publiczne	https://danepubliczne.imgw.pl/
Sea level data	GESLA v3	https://gesla787883612.wordpress.com/
Sea level data	Poseidon System	https://poseidon.hcmr.gr/services/ocean-data/situ-data
Satellite flood footprints	Global Flood Database	https://global-flood-database.cloudtostreet.ai/#interactive-map
Flood catalogue generation model	*This study*	https://doi.org/10.5281/zenodo.10678820
Modelled flood catalogue	This study	https://doi.org/10.5281/zenodo.10949631
Modelled flood footprints	This study	https://doi.org/10.5281/zenodo.10943896

References

Andreadis, K. M., O. E. Wing, E. Colven, C. J. Gleason, P. D. Bates, and C. M. Brown. 2022. Urbanizing the floodplain: Global changes of imperviousness in flood-prone areas, Environ. Res. Lett., 17, 104024. https://doi.org/10.1088/1748-9326/ac9197, 2022.

Argus, D.F., Peltier, W.R., Drummond, R., and Moore, A.W.: The Antarctica component of postglacial rebound model ICE-6G_C (VM5a) based upon GPS positioning, exposure age dating of ice thicknesses, and relative sea level histories, Geophys. J. Int., 198, 537-563, https://doi.org/10.1093/gji/ggu140, 2014.

Arnal, L., Asp, S.-S., Baugh, C., de Roo, A., Disperati, J., Dottori, F., Garcia, R., Garcia Padilla, M., Gelati, E., Gomes, G., Kalas, M., Krzeminski, B., Latini, M., Lorini, V., Mazzetti, C.,Mikulickova, M., Muraro, D., Prudhomme, C., Rauthe-Schöch, A., Rehfeldt, K., Salamon, P., Schweim, C., Skoien, J. O., Smith, P., Sprokkereef, E., Thiemig, V., Wetterhall, F., and Ziese, M.: EFAS upgrade for the extended model domain – technical documentation, Publications Office of the European Union, Luxembourg, https://doi.org/10.2760/806324, 2019.

Bates, P. D., Horritt, M. S., and Fewtrell, T. J.: A simple inertial formulation of the shallow water equations for efficient two-dimensional flood inundation modelling, J. Hydrol., 387, 33–45, https://doi.org/10.1016/j.jhydrol.2010.03.027, 2010.

Batista e Silva, F., Lavalle, C., and Koomen, E.: A procedure to obtain a refined European land use/cover map, J. Land Use Sci., 8, 255–283, https://doi.org/10.1080/1747423X.2012.667450, 2012.

Bednar-Friedl, B., Biesbroek, R., Schmidt, D.N., Alexander, P., Børsheim, K. Y., Carnicer, J., Georgopoulou, E., Haasnoot, M., Le Cozannet, G., Lionello, P., Lipka, O., Möllmann, C., Muccione, V., Mustonen, T., Piepenburg, D., and Whitmarsh, L.: Europe, Climate Change 2022: Impacts, Adaptation and Vulnerability, Contribution of Working Group II to the Sixth

Assessment Report of the Intergovernmental Panel on Climate Change, Cambridge University Press, Cambridge, UK and New York, NY, USA, 1817–1927, https://doi.org/10.1017/9781009325844.015, 2022.

Blöschl, G., Kiss, A., Viglione, A., Barriendos, M., Böhm, O., Brázdil, R., Coeur, D., Demarée, G., Llasat, M. C., Macdonald, N., Retsö, D., Roald, L., Schmocker-Fackel, P., Amorim, I., Belinová, M., Benito, G., Bertolin, C., Camuffo, D., Cornel, D., Doctor, R., Elleder, L., Enzi, S., Garcia, J. C., Glaser, R., Hall, J., Haslinger, K., Hofstätter, M., Komma, J., Limanówka, D., Lun, D., Panin, A., Parajka, J., Petric, H., Rodrigo, F. S., Rohr, C., Schönbein, J., Schulte, L., Silva, L. P., Toonen, W., Valent, P., Waser, J., and Wetter, O.: Current flood-rich period is exceptional compared to the past 500 years in Europe, Nature, 583, 560–566, https://doi.org/10.1038/s41586-020-2478-3, 2020.

Boulange, J., Hanasaki, N., Yamazaki, D., and Pokhrel, Y.: Role of dams in reducing global flood exposure under climate change, Nat Commun., 12, 417, https://doi.org/10.1038/s41467-020-20704-0, 2021.

Boyd, E., Levitan, M., and van Heerden, I.: Further specification of the dose-response relationship for flood fatality estimation, paper presented at the US-Bangladesh workshop on innovation in windstorm/storm surge mitigation construction, National Science Foundation and Ministry of Disaster & Relief, Government of Bangladesh, Dhaka, 19–21 December 2005.

Brakenridge, G. R.: Global Active Archive of Large Flood Events. Dartmouth Flood Observatory, University of Colorado, available at http://floodobservatory.colorado.edu/Archives/index.html (last access: 26 October 2023), 2023.

Burek, P., van der Knijff, J., and De Roo, A.: LISFLOOD - Distributed Water Balance and Flood Simulation Model - Revised User Manual 2013, Publications Office of the European Union, Luxembourg, https://doi.org/10.2788/24982, 2013.

Centre for Research on the Epidemiology of Disasters: EM-DAT, CRED / UCLouvain, Brussels, Belgium, https://www.emdat.be/ (last access: 26 October 2023), 2023.

Choulga, M., Moschini, F., Mazzetti, C., Grimaldi, S., Disperati, J., Beck, H., Salamon, P., and Prudhomme, C.: Technical note: Surface fields for global environmental modelling, EGUsphere [preprint], https://doi.org/10.5194/egusphere-2023-1306, 2023.

Copernicus Emergency Management Service: European Flood Awareness System (EFAS) version 5.0, available at https://confluence.ecmwf.int/display/CEMS/European+Flood+Awareness+System (last access: 8 November 2023), 2023.

Diederen, D., Liu, Y., Gouldby, B., Diermanse, F., and Vorogushyn, S.: Stochastic generation of spatially coherent river discharge peaks for continental event-based flood risk assessment, Nat. Hazards Earth Syst. Sci., 19, 1041–1053, https://doi.org/10.5194/nhess-19-1041-2019, 2019.

Dottori, F., Alfieri, L., Bianchi, A., Skoien, J., and Salamon, P.: A new dataset of river flood hazard maps for Europe and the Mediterranean Basin, Earth Syst. Sci. Data, 14, 1549–1569, https://doi.org/10.5194/essd-14-1549-2022, 2022.

Enríquez, A. R., Wahl, T., Marcos, M., and Haigh, I. D.:Spatial footprints of storm surges along the global coastlines, J. Geophys. Res.-Oceans, 125, e2020JC016367, https://doi.org/10.1029/2020JC01636, 2020.

Environment Agency: Recorded Flood Outlines, available at https://www.data.gov.uk/dataset/16e32c53-35a6-4d54-a111-ca09031eaaaf/recorded-flood-outlines (last access: 31 October 2023), 2023.

European Environment Agency: Flood phenomena, available at https://www.eea.europa.eu/data-and-maps/data/european-past-floods/flood-phenomena (last access: 26 October 2023), 2015.

European Space Agency and Sinergise: Copernicus Global Digital Elevation Model, OpenTopography [dataset], https://doi.org/10.5069/G9028PQB, 2021.

Eurostat: Statistical regions in the European Union and partner countries NUTS and statistical regions 2021 - re-edition 2022, Publications Office of the European Union, Luxembourg, https://doi.org/10.2785/321792, 2022.

Fourcy, D., and Lorvelec, O.: A new digital map of limits of oceans and seas consistent with high-resolution global shorelines, J. Coast. Res., 29, 471-477, http://dx.doi.org/10.2112/JCOASTRES-D-12-00079.1, 2013.

Frieler, K., Volkholz, J., Lange, S., Schewe, J., Mengel, M., del Rocío Rivas López, M., Otto, C., Reyer, C. P. O., Karger, D. N., Malle, J. T., Treu, S., Menz, C., Blanchard, J. L., Harrison, C. S., Petrik, C. M., Eddy, T. D., Ortega-Cisneros, K., Novaglio, C., Rousseau, Y., Watson, R. A., Stock, C., Liu, X., Heneghan, R., Tittensor, D., Maury, O., Büchner, M., Vogt, T., Wang, T., Sun, F., Sauer, I. J., Koch, J., Vanderkelen, I., Jägermeyr, J., Müller, C., Rabin, S., Klar, J., Vega del Valle, I. D., Lasslop, G., Chadburn, S., Burke, E., Gallego-Sala, A., Smith, N., Chang, J., Hantson, S., Burton, C., Gädeke, A., Li, F., Gosling, S. N., Müller Schmied, H., Hattermann, F., Wang, J., Yao, F., Hickler, T., Marcé, R., Pierson, D., Thiery, W., Mercado-Bettín, D., Ladwig, R., Ayala-Zamora, A. I., Forrest, M., and Bechtold, M.: Scenario setup and forcing data for impact model evaluation and impact attribution within the third round of the Inter-Sectoral Model Intercomparison Project (ISIMIP3a), Geosci. Model Dev., 17, 1–51, https://doi.org/10.5194/gmd-17-1-2024, 2024.

Ganguli, P., Paprotny, D., Hasan, M., Güntner, A., Merz, B.: Projected changes in compound flood hazard from riverine and coastal floods in Northwestern Europe, Earth's Future, 8, e2020EF001752, https://doi.org/10.1029/2020EF001752, 2020.

Haigh, I. D., Marcos, M., Talke, S. A., Woodworth, P. L., Hunter, J. R., and Hague, B. S.: GESLA Version 3: A major update to the global higher-frequency sea-level dataset, Geosci. Data J., 10, 293–314, https://doi.org/10.1002/gdj3.174, 2023.

Hersbach, H., Bell, B., Berrisford, P., et al.: The ERA5 global reanalysis, Q. J. R. Meteorol. Soc., 146, 1999–2049, https://doi.org/10.1002/qj.3803, 2020.

Huizinga, J., de Moel, H., Szewczyk, W.: Global flood depth-damage functions. Methodology and the database with guidelines, Publications Office of the European Union, Luxembourg, https://doi.org/10.2760/16510, 2017.

Institute of Meteorology and Water Management – National Research Institute: Dane publiczne. Available at: https://danepubliczne.imgw.pl/ (last access: 11 November 2023), 2023.

Jacob, D., Petersen, J., Eggert, B. et al.: EURO-CORDEX: new high-resolution climate change projections for European impact research, Reg. Environ. Change, 14, 563–578, https://doi.org/10.1007/s10113-013-0499-2, 2014.

Jones, P. W.: First- and Second-Order Conservative Remapping Schemes for Grids in Spherical Coordinates, Mon. Weather Rev., 127, 2204-2210, https://doi.org/10.1175/1520-0493(1999)127<2204:FASOCR>2.0.CO;2, 1999.

Jonkman, S. N., Vrijling, J. K., and Vrouwenvelder, A. C. W. M.: Methods for the estimation of loss of life due to floods: a literature review and a proposal for a new method, Nat. Hazards, 46, 353–389, https://doi.org/10.1007/s11069-008-9227-5, 2008.

Klein Goldewijk, K., Beusen, A., Doelman, J., and Stehfest, E.: Anthropogenic land use estimates for the Holocene – HYDE 3.2, Earth Syst. Sci. Data, 9, 927–953, https://doi.org/10.5194/essd-9-927-2017, 2017.

Kreibich, H., Blauhut, V., Aerts, J. C. J. H., Bouwer, L. M., Van Lanen, H. A. J., Mejia, A., Mens, M., and Van Loon, A. F.: How to improve attribution of changes in drought and flood impacts, Hydrolog. Sci. J., 64, 1–18, https://doi.org/10.1080/02626667.2018.1558367, 2019.

Kreibich, H., Schröter, K., Di Baldassarre, G., Van Loon, A. F., Mazzoleni, M., Abeshu, G. W., Agafonova, S., AghaKouchak, A., Aksoy, H., Alvarez-Garreton, C., Aznar, B., Balkhi, L., Barendrecht, M. H., Biancamaria, S., Bos-Burgering, L., Bradley, C., Budiyono, Y., Buytaert, W., Capewell, L., Carlson, H., Cavus, Y., Couasnon, A., Coxon, G., Daliakopoulos, I., de Ruiter, M. C., Delus, C., Erfurt, M., Esposito, G., François, D., Frappart, F., Freer, J., Frolova, N., Gain, A. K., Grillakis, M., Grima, J. O., Guzmán, D. A., Huning, L. S., Ionita, M., Kharlamov, M., Khoi, D. N., Kieboom, N., Kireeva, M., Koutroulis, A., Lavado-Casimiro, W., Li, H.-Y., LLasat, M. C., Macdonald, D., Mård, J., Mathew-Richards, H., McKenzie, A., Mejia, A., Mendiondo, E. M., Mens, M., Mobini, S., Mohor, G. S., Nagavciuc, V., Ngo-Duc, T., Nguyen, H. T. T., Nhi, P. T. T., Petrucci, O., Quan, N. H., Quintana-Seguí, P., Razavi, S., Ridolfi, E., Riegel, J., Sadik, M. S., Sairam, N., Savelli, E., Sazonov, A., Sharma, S., Sörensen, J., Souza, F. A. A., Stahl, K., Steinhausen, M., Stoelzle, M., Szalińska, W., Tang, Q., Tian, F., Tokarczyk, T., Tovar, C., Tran, T. V. T., van Huijgevoort, M. H. J., van Vliet, M. T. H., Vorogushyn, S., Wagener, T., Wang, Y., Wendt, D. E., Wickham, E., Yang, L., Zambrano-Bigiarini, M., and Ward, P. J.: Panta Rhei benchmark dataset: socio-hydrological data of paired events of floods and droughts, Earth Syst. Sci. Data, 15, 2009–2023, https://doi.org/10.5194/essd-15-2009-2023, 2023.

Kreibich, H., Van Loon, A. F., Schröter, K., Ward, P. J., Mazzoleni, M., Sairam, N., Abeshu, G. W., Agafonova, S., AghaKouchak, A., Aksoy, H., Alvarez-Garreton, C., Aznar, B., Balkhi, L., Barendrecht, M. H., Biancamaria, S., Bos-Burgering, L., Bradley, C., Budiyono, Y., Buytaert, W., Capewell, L., Carlson, H., Cavus, Y., Couasnon, A., Coxon, G., Daliakopoulos, I., de Ruiter, M. C., Delus, C., Erfurt, M., Esposito, G., François, D., Frappart, F., Freer, J., Frolova, N., Gain, A. K., Grillakis, M., Grima, J. O., Guzmán, D. A., Huning, L. S., Ionita, M., Kharlamov, M., Khoi, D. N., Kieboom, N., Kireeva, M., Koutroulis, A., Lavado-Casimiro, W., Li, H., Llasat, M. C., Macdonald, D., Mård, J., Mathew-Richards, H., McKenzie, A., Mejia, A., Mendiondo, E. M., Mens, M., Mobini, S., Mohor, G. S., Nagavciuc, V., Ngo-Duc, T., Nguyen, H. T. T., Nhi, P. T. T., Petrucci, O., Quan, N. H., Quintana-Seguí, P., Razavi, S., Ridolfi, E., Riegel, J., Sadik, M. S., Savelli, E., Sazonov, A., Sharma, S., Sörensen, J., Souza, F. A. A., Stahl, K., Steinhausen, M., Stoelzle, M., Szalińska, W., Tang, Q., Tian, F., Tokarczyk, T., Tovar, C., Tran, T. V. T., Van Huijgevoort, M. H. J., van Vliet, M. T. H., Vorogushyn, S., Wagener, T., Wang, Y., Wendt, D. E., Wickham, E., Yang, L., Zambrano-Bigiarini, M., Blöschl, G., and Di Baldassarre, G.: The challenge of unprecedented floods and droughts in risk management, Nature, 608, 80–86, https://doi.org/10.1038/s41586-022-04917-5, 2022.

Lange, S.: Trend-preserving bias adjustment and statistical downscaling with ISIMIP3BASD (v1.0), Geosci. Model Dev., 12, 3055–3070, https://doi.org/10.5194/gmd-12-3055-2019, 2019.

Lange, S.: ISIMIP3BASD (3.0.0), Zenodo [code], https://doi.org/10.5281/zenodo.6501284, 2022.

Le Gal, M., Fernández-Montblanc, T., Duo, E., Montes Perez, J., Cabrita, P., Souto Ceccon, P., Gastal, V., Ciavola, P., and Armaroli, C.: A new European coastal flood database for low–medium intensity events, Nat. Hazards Earth Syst. Sci., 23, 3585–3602, https://doi.org/10.5194/nhess-23-3585-2023, 2023.

Lehner, B., Reidy Liermann, C., Revenga, C., Vörösmarty, C., Fekete, B., Crouzet, P., Döll, P., Endejan, M., Frenken, K., Magome, J., Nilsson, C., Robertson, J. C., Rodel, R., Sindorf, N., and Wisser, D.: High-resolution mapping of the world's reservoirs and dams for sustainable river-flow management, Front. Ecol. Environ., 9, 494-502, https://doi.org/10.1890/100125, 2011.

Lyard, F. H., Allain, D. J., Cancet, M., Carrère, L., and Picot, N.: FES2014 global ocean tide atlas: design and performance, Ocean Sci., 17, 615–649, https://doi.org/10.5194/os-17-615-2021, 2021.

Mengel, M., Treu, S., Lange, S., and Frieler, K.: ATTRICI v1.1 – counterfactual climate for impact attribution, Geosci. Model Dev., 14, 5269–5284, https://doi.org/10.5194/gmd-14-5269-2021, 2021.

Mentaschi, L., Vousdoukas, M., Voukouvalas, E., Sartini, L., Feyen, L., Besio, G., and Alfieri, L.: The transformed-stationary approach: a generic and simplified methodology for non-stationary extreme value analysis, Hydrol. Earth Syst. Sci., 20, 3527–3547, https://doi.org/10.5194/hess-20-3527-2016, 2016.

Merz, B., Blöschl, G., Vorogushyn, S., Dottori, F., Aerts, J. C., Bates, P., Bertola, M., Kemter, M., Kreibich, H., and Lall, U.: Causes, impacts and patterns of disastrous river floods, Nature Reviews Earth & Environment, 2, 592–609, https://doi.org/10.1038/s43017-021-00195-3, 2021.

Mester, B., Frieler, K., and Schewe, J.: Human displacements, fatalities, and economic damages linked to remotely observed floods, Sci. Data, 10, 482, https://doi.org/10.1038/s41597-023-02376-9, 2023.

Muis, S., Apecechea, M. I., Dullaart, J., de Lima Rego, J., Madsen, K. S., Su, J., Yan, K., and Verlaan, M.: A High-resolution global dataset of extreme sea levels, tides, and storm surges, including future projections, Frontiers in Marine Science, 7, 263, https://doi.org/10.3389/fmars.2020.00263, 2020.

Mulet, S., Rio, M.-H., Etienne, H., Artana, C., Cancet, M., Dibarboure, G., Feng, H., Husson, R., Picot, N., Provost, C., and Strub, P. T.: The new CNES-CLS18 global mean dynamic topography, Ocean Sci., 17, 789–808, https://doi.org/10.5194/os-17-789-2021, 2021.

Muñoz-Sabater, J., Dutra, E., Agustí-Panareda, A., Albergel, C., Arduini, G., Balsamo, G., Boussetta, S., Choulga, M., Harrigan, S., Hersbach, H., Martens, B., Miralles, D. G., Piles, M., Rodríguez-Fernández, N. J., Zsoter, E., Buontempo, C., and Thépaut, J.-N.: ERA5-Land: a state-of-the-art global reanalysis dataset for land applications, Earth Syst. Sci. Data, 13, 4349–4383, https://doi.org/10.5194/essd-13-4349-2021, 2021.

Nicholls, R. J., Lincke, D., Hinkel, J., Brown, S., Vafeidis, A. T., Meyssignac, B., Hanson, S. E., Merkens, J. L., and Fang, J.: A global analysis of subsidence, relative sea-level change and coastal flood exposure, Nat. Clim. Change, 11, 338–342, https://doi.org/10.1038/s41558-021-00993-z, 2021.

Papagiannaki, K., Petrucci, O., Diakakis, M., Kotroni, V., Aceto, L., Bianchi, C., Brázdil, R., Gelabert, M. G., Inbar, M., Kahraman, A., Kılıç, Ö., Krahn, A., Kreibich, H., Llasat, M. C., Llasat-Botija, M., Macdonald, N., de Brito, M. M., Mercuri, M., Pereira, S., Řehoř, J., Geli, J. R., Salvati, P., Vinet, F., Zêzere, J. L.: Developing a large-scale dataset of flood fatalities for territories in the Euro-Mediterranean region, FFEM-DB, Sci. Data, 9, 166, https://doi.org/10.1038/s41597-022-01273-x, 2022.

Paprotny, D. and Morales-Nápoles, O.: Estimating extreme river discharges in Europe through a Bayesian network, Hydrol. Earth Syst. Sci., 21, 2615-2636, doi:10.5194/hess-21-2615-2017, 2017

Paprotny, D., Mengel, M.: Population, land use and economic exposure estimates for Europe at 100 m resolution from 1870 to 2020, Sci. Data, 10, 372, https://doi.org/10.1038/s41597-023-02282-0, 2023.

Paprotny, D., Morales Nápoles, O., Nikulin, G.: Extreme sea levels under present and future climate: a pan-European database, E3S Web of Conferences, 7, 02001, https://doi.org/10.1051/e3sconf/20160702001, 2016.

Paprotny, D., Morales Nápoles, O., Vousdoukas, M. I., Jonkman, S. N., and Nikulin, G.: Accuracy of pan-European coastal flood mapping, J. Flood Risk Manag., 12(2), e12459, https://doi.org/10.1111/jfr3.12459, 2019.

Paprotny, D., Morales-Nápoles, O., and Jonkman, S. N.: Efficient pan-European river flood hazard modelling through a combination of statistical and physical models, Nat. Hazards Earth Syst. Sci., 17, 1267–1283, https://doi.org/10.5194/nhess-17-1267-2017, 2017.

Paprotny, D., Morales-Nápoles, O., and Jonkman, S. N.: HANZE: a pan-European database of exposure to natural hazards and damaging historical floods since 1870, Earth Syst. Sci. Data, 10, 565–581, https://doi.org/10.5194/essd-10-565-2018, 2018a.

Paprotny, D., Sebastian, A., Morales Nápoles, O., and Jonkman, S. N.: Trends in flood losses in Europe over the past 150 years, Nat. Commun., 9, 1985, https://doi.org/10.1038/s41467-018-04253-1, 2018b.

Paprotny, D., Terefenko, P., and Śledziowski, J.: An improved database of flood impacts in Europe, 1870–2020: HANZE v2.1, Earth Syst. Sci. Data Discuss. [preprint], https://doi.org/10.5194/essd-2023-321, in review, 2023.

Paprotny, D.: HANZE catalogue of modelled and historical floods in Europe, 1950-2020 [dataset], https://doi.org/10.5281/zenodo.10629443, 2024.

Paprotny D., 't Hart C. M. P., Morales-Napoles O.: Evolution of flood protection levels and flood vulnerability in Europe since 1950 estimated with vine-copula models, Research Square [preprint], in review, https://doi.org/10.21203/rs.3.rs-4213746/v1, 2024.

Peltier, W.R., Argus, D.F., and Drummond, R.: Space geodesy constrains ice-age terminal deglaciation: The global ICE-6G_C (VM5a) model, J. Geophys. Res. Solid Earth, 120, 450-487, https://doi.org/10.1002/2014JB011176, 2015.

Poseidon System: Monitoring, forecasting and information system for the Greek seas, available at https://poseidon.hcmr.gr/. Last accessed 16 January 2024.

Pronk, M., Hooijer, A., Eilander, D., Haag, A., de Jong, T., Vousdoukas, M., Vernimmen, R., Ledoux, H., Eleveld, M.: DeltaDTM: A global coastal digital terrain model, Sci. Data, 11, 273, https://doi.org/10.1038/s41597-024-03091-9, 2024.

Pujol, M.-I., Faugère, Y., Taburet, G., Dupuy, S., Pelloquin, C., Ablain, M., and Picot, N.: DUACS DT2014: the new multi-mission altimeter data set reprocessed over 20 years, Ocean Sci., 12, 1067–1090, https://doi.org/10.5194/os-12-1067-2016, 2016.

Rentschler, J., Avner, P., Marconcini, M., Su, R., Strano, E., Vousdoukas, M., and Hallegatte, S.: Global evidence of rapid urban growth in flood zones since 1985, Nature, 622, 87–92, https://doi.org/10.1038/s41586-023-06468-9, 2023.

Rojas, R., Feyen, L., and Watkiss, P.: Climate change and river floods in the European Union: Socio-economic consequences and the costs and benefits of adaptation. Glob. Environ. Change, 23, 1737–1751. https://doi.org/10.1016/j.gloenvcha.2013.08.006, 2013.

Sauer, I., Reese, R., Otto, C., Geiger, T., Willner, S., Guillod, B. P., Bresch, D. N., and Frieler, K.: Climate signals in river flood damages emerge under sound regional disaggregation. Nat. Commun., 12, 2128, https://doi.org/10.1038/s41467-021-22153-9, 2021.

Schoppa, L., Barendrecht, M. H., Paprotny, D., Sairam, D., Sieg, T., and Kreibich, H.: Projecting Flood Risk Dynamics for Effective Long-term Adaptation, Earth's Future, 12, e2022EF003258, https://doi.org/10.1029/2022EF003258, 2024.Scussolini, P., Luu, L. N., Philip, S. Y., Berghuijs, W. R., Eilander, D., Aerts, J. C. J. H., Kew, S. F., van Oldenborgh, G. J., Toonen, W. H. J., Volkholz, J., Coumou, D.: Challenges in the attribution of river flood events, WIREs Climate Change, e874. https://doi.org/10.1002/wcc.874, 2023.

Steinhausen, M., Paprotny, D., Dottori, F., Sairam, N., Mentaschi, L., Alfieri, L., Lüdtke, S., Kreibich, H., and Schröter K.: Drivers of future fluvial flood risk change for residential buildings in Europe, Global Environ. Chang., 76, 102559, https://doi.org/10.1016/j.gloenvcha.2022.102559, 2022.

Taburet, G., Sanchez-Roman, A., Ballarotta, M., Pujol, M.-I., Legeais, J.-F., Fournier, F., Faugere, Y., and Dibarboure, G.: DUACS DT2018: 25 years of reprocessed sea level altimetry products, Ocean Sci., 15, 1207–1224, https://doi.org/10.5194/os-15-1207-2019, 2019.

Tellman, B., Sullivan, J. A., Kuhn, C., Kettner, A. J., Doyle, C. S., Brakenridge, G. R., Erickson, T. A., and Slayback, D. A.: Satellite imaging reveals increased proportion of population exposed to floods, Nature, 596, 80–86, https://doi.org/10.1038/s41586-021-03695-w, 2021.

Thiemig, V., Gomes, G. N., Skøien, J. O., Ziese, M., Rauthe-Schöch, A., Rustemeier, E., Rehfeldt, K., Walawender, J. P., Kolbe, C., Pichon, D., Schweim, C., and Salamon, P.: EMO-5: a high-resolution multi-variable gridded meteorological dataset for Europe, Earth Syst. Sci. Data, 14, 3249–3272, https://doi.org/10.5194/essd-14-3249-2022, 2022.

Tilloy, A., Paprotny, D., Grimaldi, S., Gomes, G., Bianchi, A., Lange, S., Beck, H., and Feyen, L.: HERA: a high-resolution pan-European hydrological reanalysis (1950–2020), Earth Syst. Sci. Data Discuss. [preprint], https://doi.org/10.5194/essd-2024-41, in review, 2024.

Treu, S., Muis, S., Dangendorf, S., Wahl, T., Oelsmann, J., Heinicke, S., Frieler, K., and Mengel, M.: Reconstruction of hourly coastal water levels and counterfactuals without sea level rise for impact attribution, Earth Syst. Sci. Data, 16, 1121–1136, https://doi.org/10.5194/essd-16-1121-2024, 2024.

U.S. Army Corps of Engineers: Coastal Engineering Manual, EM 1110-2-1100, Department of the Army, Washington D.C., 2002.

van der Knijff, J.: LISVAP– Evaporation Pre-Processor for the LISFLOOD Water Balance and Flood Simulation Model, User Manual, Office for Official Publications of the European Communities, Luxembourg, https://dx.doi.org/10.2788/26160, 2006.

Vogt, J.V., Soille, P., De Jager, A., Rimaviciute, E., Mehl, W., Foisneau, S., Bodis, K., Dusart, J., Paracchini, M., Haastrup, P., and Bamps, C.: A pan-European River and Catchment Database, Publications Office of the European Union, Luxembourg, https://dx.doi.org/10.2788/35907, 2007.

Vousdoukas, M. I., Athanasiou, P., Giardino, A., Mentaschi, L., Stocchino, A., Koop, R. E., Menéndez, P., Beck, M. W., Ranasinghe, R., and Feyen, L.: Small Island Developing States under threat by rising seas even in a 1.5 °C warming world, Nat. Sustain., https://doi.org/10.1038/s41893-023-01230-5, 2023.

Vousdoukas, M. I., Mentaschi, L., Voukouvalas, E., Bianchi, A., Dottori, F., and Feyen, L.: Climatic and socioeconomic controls of future coastal flood risk in Europe, Nat. Clim. Change, 8, 776-780, https://doi.org/10.1038/s41558-018-0260-4, 2018.

Vousdoukas, M. I., Mentaschi, L., Voukouvalas, E., Verlaan, M., and Feyen, L.: Extreme Sea levels on the rise along Europe's coasts, Earth's Future, 5, 304–323, https://doi.org/10.1002/2016ef000505, 2017.

Vousdoukas, M. I., Voukouvalas, E., Annunziato, A., Giardino, A., and Feyen, L.: Projections of extreme storm surge levels along Europe. Climate Dynamics, 47, 3171-3190, https://doi.org/10.1007/s00382-016-3019-5, 2016a.

Vousdoukas, M. I., Voukouvalas, E., Mentaschi, L., Dottori, F., Giardino, A., Bouziotas, D., Bianchi, A., Salamon, P., and Feyen, L.: Developments in large-scale coastal flood hazard mapping, Nat. Hazards Earth Syst. Sci., 16, 1841–1853, https://doi.org/10.5194/nhess-16-1841-2016, 2016b.

Wada, Y., Flörke, M., Hanasaki, N., Eisner, S., Fischer, G., Tramberend, S., Satoh, Y., van Vliet, M. T. H., Yillia, P., Ringler, C., Burek, P., and Wiberg, D.: Modeling global water use for the 21st century: the Water Futures and Solutions (WFaS) initiative and its approaches, Geosci. Model Dev., 9, 175–222, https://doi.org/10.5194/gmd-9-175-2016, 2016.

Wing, O. E. J., Smith, A. M., Marston, M. L., Porter, J. R., Amodeo, M. F., Sampson, C. C., and Bates, P. D.: Simulating historical flood events at the continental scale: observational validation of a large-scale hydrodynamic model, Nat. Hazards Earth Syst. Sci., 21, 559–575, https://doi.org/10.5194/nhess-21-559-2021, 2021.

Zanaga, D., Van De Kerchove, R., De Keersmaecker, W., Souverijns, N., Brockmann, C., Quast, R., Wevers, J., Grosu, A., Paccini, A., Vergnaud, S., Cartus, O., Santoro, M., Fritz, S., Georgieva, I., Lesiv, M., Carter, S., Herold, M., Li, Linlin, Tsendbazar, N.E., Ramoino, F., Arino, O.: ESA WorldCover 10 m 2020 v100 [dataset], https://doi.org/10.5281/zenodo.5571936, 2021.